

# 6 Zero-Variance Theory for Efficient Subsurface Scattering

Eugene d’Eon and Jaroslav Křivánek<sup>1</sup>

## 6.1 Introduction

The topic of this chapter is *zero-variance Monte Carlo schemes* and their use for improving the convergence rates of Monte Carlo subsurface scattering (SSS) calculations for image synthesis. We expand upon a previous work by the authors [Křivánek and d’Eon 2014] and include several new result such as

- Two new perfectly-zero-variance half-space escape schemes,
- Zero-variance theory for generalized radiative transfer (GRT) (non-exponential random media),
- An exit-resampling procedure for asymptotic/Dwivedi guiding that better accounts for the importance change near boundaries.

### 6.1.1 Brute Force Subsurface Scattering

Brute force Monte Carlo subsurface scattering is now commonplace in production rendering software [Chiang et al. 2016; Kulla et al. 2018; Fascione et al. 2018; Christensen et al. 2018; Georgiev et al. 2018]. This approach works by sampling random walks/flights inside a participating medium to connect illuminated surface points to nearby exit points (Figure 1). These random walks are unbiased Monte Carlo estimators of fully general *bidirectional scattering-surface reflectance-distribution functions* (BSSRDFs) [Nicodemus et al. 1977] and so are highly flexible and accurate. However, they can be considerably slower than methods that use approximate BSSRDFs. In this chapter we show how analytic importance functions can be used to guide the sampling of these random walks such that the efficiency of the method is improved without losing accuracy.

The BSSRDF is what gives rise to the characteristic bleeding of light that makes translucent materials like human skin appear soft. High quality predictive image synthesis requires that the BSSRDFs are accurately specified and sampled. However, in contrast to BRDFs that are typically known analytically, in any practical setting the BSSRDF is a high-dimensional and *unknown* function. This is because it follows from the solution to an integral equation for the collision density inside the material and that solution depends on the shape of the boundary. The boundary, and therefore the BSSRDF, might even change over time—the BSSRDF of your nose changes as you wiggle your toes (although not measurably). Even in idealized scenarios where exact solutions are known [Williams 2007; Machida et al. 2010; Liemert and Kienle 2013], they are only known in a semi-analytic form and exhibit no obvious importance sampling scheme for generating outgoing surface positions and directions in a single step. Approximate BSSRDFs can be sampled very efficiently, however, but at the cost of accuracy.

Most efficient SSS algorithms proposed in graphics [Jensen et al. 2001; Borshukov and Lewis 2003; Donner and Jensen 2005; d’Eon et al. 2007; Donner et al. 2008; D’Eon and Irving 2011; Christensen 2015] approximate the BSSRDF with a 2D lateral convolution of the incident light based on solutions of the transport equation in plane geometry and then impose diffusive angular shapes on the outgoing radiance. Later methods have improved upon the angular domain of this approach [Habel et al. 2013; d’Eon 2014; Frisvad et al. 2014; Frederickx and Dutré 2017], but lack the general accuracy and flexibility of the random walk approach in curved geometry. With increasing compute power the trend is more and more in favour of exact BSSRDFs that satisfy the equation of radiative transfer.

---

<sup>1</sup>This chapter contains novel material by both authors that was regrettably not published before Jaroslav’s passing. As such, it is essential that any reference to this work includes attribution to Jaroslav.

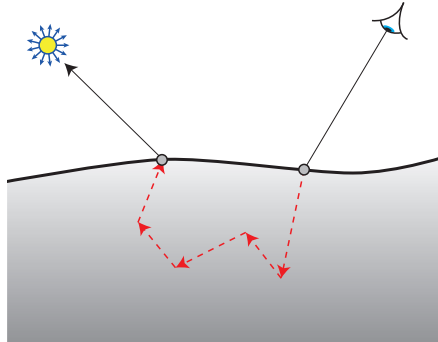


**Figure 1:** Random-walk SSS can result in long complex paths (illustrated here as dashed lines) inside the material that transport light beneath the surface from a point of illumination to some nearby location. The standard methods for sampling these paths can result in high variance weights due to longer paths being absorbed more. This chapter discusses guided sampling techniques that reduce this variance, yielding faster convergence, shorter paths on average, and, therefore, shorter render times.

Despite not knowing the exact BSSRDF itself, we always have a simple Monte Carlo procedure for importance sampling it: the random walk is generated from alternate sampling of the free-path-length distribution (moving the position of the walk) and phase function (changing the walk’s direction) until escape is sampled (with BSDF sampling at the boundary). This procedure follows directly from the integral equation that the collision rate density inside the material satisfies [Lafortune and Willems 1996; Raab et al. 2008]. This flexible approach works regardless of the shape of the object, how scattering and absorption processes inside vary, or what BSDF is on the boundary.

In the absence of absorption inside the volume, the classical random walk method is already *zero variance*—every path is sampled in exact proportion to the BSSRDF with unit weight (assuming nothing inside or on the boundary absorbs light). For such impossibly-white materials, the content in this chapter has nothing to offer. When absorption is present, however, the weights of this sampling procedure vary with  $\alpha^n$  where  $\alpha$  is the *single-scattering albedo* at each collision event and  $n$  is the number of medium collisions along the path (the number of times the phase function is sampled). The main objective of applying zero-variance schemes to random walk SSS is to remove all variance in the path weight that is due to internal absorption. Because of the plane-parallel nature of the guiding, these methods also apply directly to stochastic methods for sampling layered materials using “position-free” walks [Hanrahan and Krueger 1993; Guo et al. 2018].

### 6.1.2 Terminology

Much of the zero-variance theory that we apply originates from the neutron transport literature [Kahn 1956; Coveyou et al. 1967; Hoogenboom 2008a]. In this literature, statistically unbiased estimators that converge to the correct answer are referred to as “fair games”, and an estimator “scores” a value (its final particle weight, usually). The term “analog” sampling refers to always *locally* sampling free-path distributions and phase functions directly from their given distributions in isolation, oblivious to where light sources or camera sensors lie in the scene. As such, the simulated particle does the physical analog of a real particle in a physical system [Spanier and Gelbard 1969]. In analog sampling, the particle weight is always 1 (continue to scatter) or 0 (death by absorption, terminating the walk).

In the context of rendering, analog sampling is only implicitly used for materials like glass and mirrors that do not lose any energy. The analog sampling of other BSDFs like a Lambertian reflector would sample outgoing directions and terminate the particle with a probability equal to one minus the diffuse

albedo (equivalent to Russian Roulette that always ensure unit particle weight). Instead, we almost always directly jump to using “Implicit capture”—a form of variance reduction that uses a statistical particle weight to account for absorption. In a participating medium, for example, this works by adjusting the particle weight by a factor of the single-scattering albedo  $\alpha$  at every collision. When we refer to “classical sampling”, we mean analog sampling plus implicit capture, which is technique described in graphics text books [Pharr et al. 2016].

In the neutron transport literature, “biased” can refer to importance sampling anything other than the analog distributions. When this literature refers to, for example, “biased direction sampling” in the context of zero-variance theory, they are simply referring to drawing directions from a distribution other than the phase function and adopting the appropriate weight adjustment to ensure a “fair game”. We will instead use “guiding”, to avoid any confusion with “statistical bias”.

We will limit our attention to BSSRDF sampling alone and not to the challenging task of sampling the product of incident illumination with the BSSRDF. This is equivalent to assuming a uniform isotropic source everywhere on the boundary surface and we use the term “guiding-to-escape” for this class of problem. However, the same general theory applies (with higher-dimensional importance functions) to guide SSS random walks when the incident illumination at the boundary is known both in the angular and spatial domains. In this case, it is common to use a two-stage procedure where an approximate importance function is predetermined in the volume in some discrete form either using deterministic or Monte Carlo methods before random walks begin [Turner and Larsen 1997].

We will follow neutron transport and use “collision” to refer to interactions with the medium, which includes both absorbing and scattering collisions.

### 6.1.3 Outline

Our main goal in this course is to complement the theoretical literature on zero variance schemes by working through several examples that clearly illustrate how the theory is applied in practice. A secondary motivation is to show how the theory can be applied in random media (GRT). After reviewing related work in the next section we define and motivate GRT in Section 6.3. Several key differences between classical and non-exponential (non-Beerian) transport are discussed before defining the general framework of escaping a half space with isotropic scattering in GRT (Section 6.4). In Section 6.5 we derive two new exactly-zero-variance random walks, one for classical scattering in a rod and one for a closely related problem of Gamma-2 random flights in 3D. These examples not only demonstrate that exactly zero variance walks are possible, but also illustrate how such walks differ from classical unguided walks, and how the notion of adjoint importance (exact or approximate) is used to product sample free-path-length and angle sampling decisions to guide a random walk towards a zero-variance version. We review asymptotic (Dwivedi) guiding in Section 6.6 and discuss anisotropic scattering. We finish with some general tips (Section 6.7).

## 6.2 Related Work

We recommend Hoogenboom [2008a] for a thorough review of the history of zero variance theory including a complete treatment of last-event, collision and track-length estimators. We also recommend Turner and Larsen [1997] for additional details, but prefer the integral equation approach of Hoogenboom, not only because the integro-differential form gets messy, but mostly because of its natural fit for GRT. The related *contributon* theory is also worth noting [Williams 1991].

For a survey of methods that use deterministic importance functions for particle guiding, see [Haghigat and Wagner 2003].

**Deep-Penetration Monte Carlo** The primary motivation for analytical zero-variance estimators is for shielding calculations in particle transport where the variance reduction for guided vs unguided

walks is many orders of magnitude and the guiding is, on average, towards deeper locations in the material, as opposed to subsurface scattering, where we guide to escape the volume anywhere, although typically back towards the entry location. For a recent survey on variance reduction methods for deep-penetration neutron transport, see [Munk and Slaybaugh 2019].

**Condensed History** There are several other ways to improve the efficiency of the random walk approach to SSS. Similarity theory and condensed-history schemes can be used to progressively alter the analog sampling distributions as the walk is generated in order to simulate more than one propagation step at a time (for example, making the phase function more isotropic after some number of events, and adjusting the future mean free path to compensate). In doing this, the history of the particle is condensed into fewer individual steps. These methods often introduce small errors, but some aspects of these schemes can exactly maintain desired properties of the uncondensed transport. Condensed history schemes are highly effective in infinite media, but handling boundary crossing/escape without significant error is a major challenge.

A variety of condensed history schemes called *shell-tracing* (in computer graphics [Müller et al. 2016]) begins by finding the largest sphere around a previous collision such that the medium can be considered homogeneous inside that sphere. The particle is then teleported to that sphere's surface with an appropriate weight adjustment [Fleck and Canfield 1984; Moon et al. 2007]. For some problems this can yield massive gains.

Both condensed history and similarity theory have the most to offer in weakly absorbing materials where thousands of collisions per walk are common, whereas zero-variance guiding-to-escape schemes provide more relative benefit when the material absorbs, making the two approaches complementary. They can be combined using the same steps outlined in this chapter by normalizing the appropriate product involving the importance function. For use of similarity theory in graphics see [Frisvad et al. 2007; Zhao et al. 2014]. For more on condensed history see [Bhan and Spanier 2007; d'Eon 2016].

**Guiding and Importance in Graphics** The zero-variance Monte Carlo theory is tightly coupled to the theory of adjoint estimators and importance. See Christensen [2003] for an excellent summary of the use of adjoint importance in graphics. We also note several works [Xu et al. 2001; Xu et al. 2006] that applied the zero variance theory explicitly for global illumination in scenes with no participating media.

**Machine Learning** Several recent works have used machine learning to directly importance sample BSSRDFs on curved domains [Vicini et al. 2019] and to accelerate subsurface transport using learned infinite medium Green's functions [Deng et al. 2020]. Almost certainly we will see more applications involving machine learning to path guiding in volumes. We hope that some of the deterministic principles that we touch upon in this chapter will inform the design of these methods.

### 6.3 Generalized Radiative Transfer (GRT)

The transport of waves or particles in a random medium consisting of optically active particles/microstructure is sensitive to exactly how these particles are distributed. When particles in a region with a fixed number density are reconfigured to obey positive (clumpy) or negative (repelling) spatial correlation, this will give rise to different attenuation laws and bulk transport (Figure 2). This phenomena has been long recognized under a variety of names, such as the *sieve/package effect* [Rabinowitch 1951; Kirk 1975], the *channeling effect* [Burrs 1958; Burrs 1960], *distributional error* [Fukshansky 1987], or *large scale inhomogeneities, clumping, mixing-fraction variations, particle-self-shielding* [Randall 1962]. Particle reconfiguration can completely transform the properties of the material from transparent to opaque [Torquato 2016]. It is desirable to formulate transport theory machinery that can efficiently account for these effects in order to simulate the broadest class of materials.

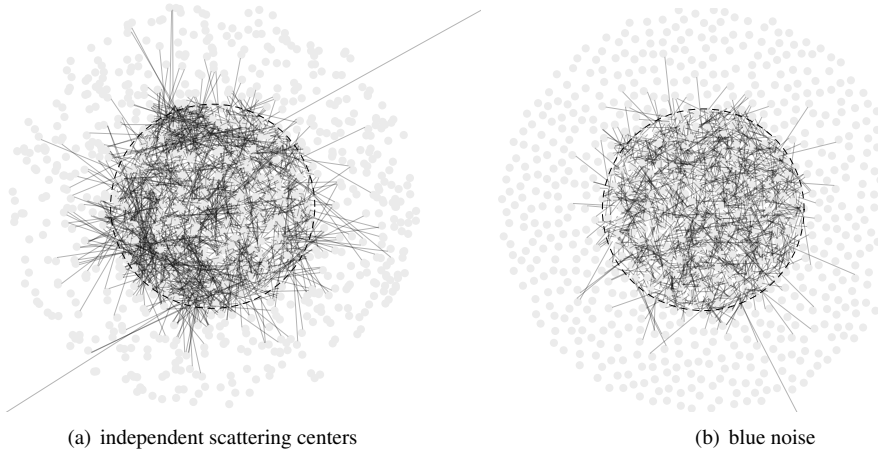


**Figure 2:** The same density of particles reconfigured from an independent distribution (left) to a configuration with negative (repelling) correlation yields shorter mean free paths. Here we show 2000 paths in each image with origins drawn uniformly from the dashed circle extended to their first collision.

The gold standard approach for including distributional effects in random media is with a stochastic transport equation that permits the material coefficients to become random variables. This approach was first applied in wave transport [Frisch 1968; Ishimaru 1978], and later to the scalar equation of radiative transfer [Anisimov and Fukshansky 1992]. Solving for the mean transport over all permissible random realizations of the system with an averaging step is a rigorous approach but it is challenging to derive exact solutions from this method without making additional assumptions about the magnitude of the correlations. The corresponding rigorous Monte Carlo approach is called *quenched disorder* [Larmier et al. 2017] and works by sampling a number of explicit random realizations for the medium and then performing classical (deterministic or Monte Carlo) transport calculations within each. The desired transport quantities are averaged over the simulated realizations. This approach is also prohibitively expensive and neither of these rigorous approaches is likely to be directly applied in computer graphics. However, both are important benchmarking tools that can be used to evaluate faster approximate methods.

One highly efficient approach to approximating the stochastic transfer equation is to adopt a short term memory and only remember enough of the past to exactly exhibit the free-path-length statistics between collisions [Randall 1964; Hoffman 1964; Audic and Frisch 1993; Moon et al. 2007; Larsen and Vasques 2011]. This is the foundation of what we will refer to as *generalized radiative transfer* (GRT) [d’Eon 2019a; Davis and Xu 2014]. This allows a new aspect of random media that classical transport theory lacks, which is that the distribution of *free-path-lengths between collisions*  $p_c(s)$  can be non-exponential (and the attenuation law non-Beerian). This distribution can be measured from Monte Carlo simulation in quenched disorder [Audic and Frisch 1993; Moon et al. 2007; Larsen and Vasques 2011] or from analytical analysis of a given stochastic model for the random extinction coefficient  $\mu_t$  [Davis and Mineev-Weinstein 2011]. The stochastic process of a particle moving through the system is then a continuous time random walk [Weiss 1983] or, from a time-independent viewpoint, simply a general random flight based on  $p_c(s)$  [Dutka 1985].

To apply zero variance theory to GRT we need a transport equation. Two equivalent such equations are known. The integro-differential-like equation of GRT includes a time-like integration over a memory variable  $s$ —the distance since the previous medium or boundary interaction [Larsen and Vasques 2011].

This increases the phase space of transport with an extra dimension. This memory is required to exhibit the semi-Markov nature of the particle flight. From a discrete-time point of view (over collision order), the collision chain is fully Markovian, and the collision-rate density satisfies a generalized Peierls's integral equation [Grosjean 1951; d'Eon 2019a]. This is the simpler equation of transfer, closest to the classical form, where all memory is encoded in  $p_c(s)$ , and from this the zero variance theory is immediately applicable. These integral equations have been used to generalize the volume rendering equation in computer graphics [d'Eon 2013; Jarabo et al. 2018; Bitterli et al. 2018].

To summarize, GRT is a non-exponential random flight where intercollision free path lengths are drawn from  $p_c(s)$ , and absorption and scattering are non-stochastic (do not depend on  $s$ ). The attenuation law when leaving a collision is then [Larsen and Vasques 2011]

$$X_c(s) = \int_s^\infty p_c(s')ds'. \quad (1)$$

We require a second set of statistics to apply GRT to bounded domains in a form that satisfies Helmholtz reciprocity. This follows from the need to distinguish between stochastic and deterministic origins in GRT [Audic and Frisch 1993]. Consider the mean chord length between particles in the medium over various realizations. We can only begin such paths from an origin where the last collision ended. Thus, we average over only those realizations with a particle at the origin. This origin is then *correlated* to the other particles in the volume and we use the label "c". In contrast, a deterministic location on a material boundary lies in all realizations of the system. The statistics for free-path length from the boundary must average over the full ensemble (these path-lengths are not chords [Lu and Torquato 1992]). This leads to a related distribution  $p_u(s)$  for the *free-path-lengths to next collision from an uncorrelated origin*. The distribution  $p_u(s)$  is used for any path leaving a boundary surface or emission from the volume in an uncorrelated manner. Otherwise  $p_c(s)$  is used and the two distributions only align for the unique case of exponential random media  $p_c(s) = p_u(s) = e^{-s/\ell}/\ell$ , where  $\ell$  is the *mean free path*. There is a related attenuation law from uncorrelated origins given by

$$X_u(s) = \int_s^\infty p_u(s')ds'. \quad (2)$$

For an example illustrating why the two distributions differ, see Figure 3.

If any one of  $p_c(s)$ ,  $p_u(s)$ ,  $X_c(s)$ ,  $X_u(s)$  are known, the other three are uniquely determined by simple relations [d'Eon 2018]. The distribution  $p_u(s)$  is also known as the equilibrium distribution of free path lengths, and  $X_c(s)$  and  $p_u(s)$  are proportional [Feller 1971; Tunaley 1974; Tunaley 1976; Weiss 1983].

### 6.3.1 Radiance and Collision Density

An important distinction between two fundamental transport quantities arises in GRT due to the breaking of their classical local proportionality: radiance and collision rate density [d'Eon 2013]. Radiance  $L(\mathbf{x}, \omega)$  describes the density of particles *in flight* at position  $\mathbf{x}$  in direction  $\omega$ . This tells us what we would measure if we inserted a tiny camera sensor in the volume and let particles hit that detector. This measurement is of the particles in flight, not the scatterers in the medium. The collision rate density  $C(\mathbf{x}, \omega)$  is defined such that  $C(\mathbf{x}, \omega)d\omega d\mathbf{x}$  is the rate at which particles are entering collisions within positions  $d\mathbf{x}$  about  $\mathbf{x}$  and confined to directions in  $d\omega$  about  $\omega$ . Measuring this quantity is to observe the medium itself: the scatterers. Only in classical exponential media do we find the *local* proportionality

$$C(\mathbf{x}, \omega) = \mu_t(\mathbf{x}, \omega)L(\mathbf{x}, \omega). \quad (3)$$

In GRT, the extinction coefficient  $\mu_t(s) = p_c(s)/X_c(s)$  is not a locally defined quantity, and so no local conversion is possible. Volumes in GRT are therefore specified with  $p_c(s)$ , albedo  $\alpha$  and phase function  $P$ , as opposed to absorption and scattering coefficients.

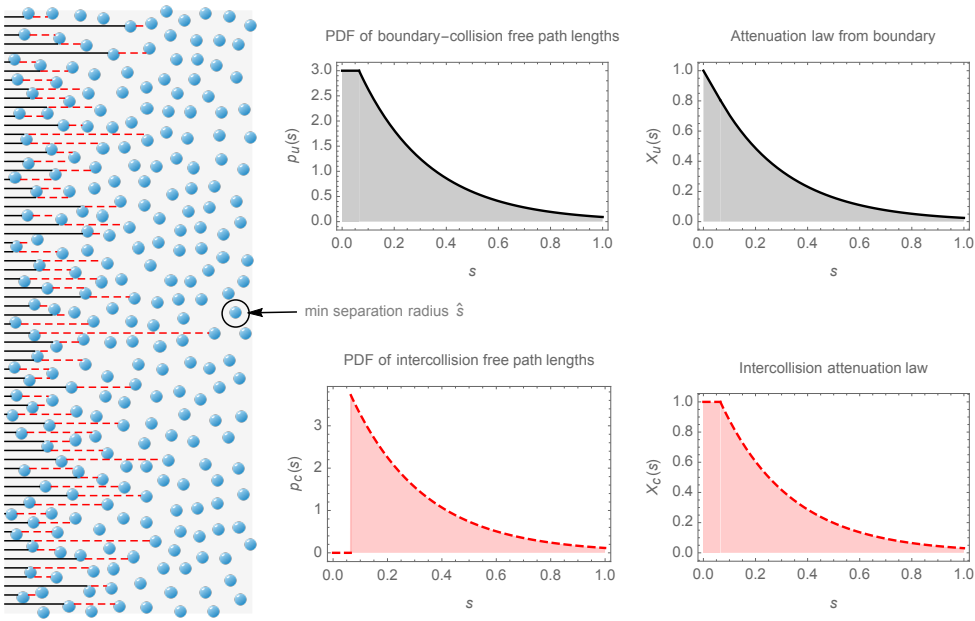


**Figure 3:** When scatterers in a random medium are spatially correlated, the free-path length statistics between collisions are necessarily distinct from those for paths beginning at a boundary interface. Here we illustrate the case of negatively-correlated convex scatterers separated by a minimum distance  $\hat{s} = 0.065$ . For paths beginning at the left boundary of a unit thickness slab (solid-black) collisions can occur arbitrarily close to the boundary and the related path length PDF  $p_u(s)$  and attenuation law  $X_u(s)$  reflect this. Continuing in the same direction from the first collision to the second collision (red-dashed), we find path lengths with a minimum length  $\hat{s}$ . The intercollision free-path distribution  $p_c(s)$  is therefore identically zero for  $s < \hat{s}$  due to the scatterers separation, and the attenuation law between collisions  $X_c(s)$  is 1 for this initial distance. Note that  $X_c(s)$  and  $p_u(s)$  are always proportional.

Because of the new relationship between radiance and collision density in GRT (and their scalar counterparts, fluence and scalar collision density  $C(\mathbf{x})$ ), generalization of classical methods require extra care. Each of these quantities has distinct collision and track-length estimators and diffusion approximations in GRT, where in the classical case there was effectively only one form of these tools [d'Eon 2019a]. This is important to keep in mind with respect to graphics literature where the integral equation inside of volumes is always written over radiance

$$L(\mathbf{x}, \omega) = \int_0^\infty X_c(s) \int_{4\pi} \mu_s P(\omega' \rightarrow \omega) L(\mathbf{x} - s\omega, \omega') d\omega' ds \quad (4)$$

probably for the reason that radiance is the quantity at the camera aperture that forms the final image. However, it is only the collisions in the volume that the camera sees, not all the particles in flight, and so the integral equation for collision density is more directly tied to what we integrate in volumetric path tracing

$$L(\mathbf{x}, \omega) = \int_0^\infty X_c(s) \int_{4\pi} \alpha P(\omega' \rightarrow \omega) C(\mathbf{x} - s\omega, \omega') d\omega' ds \quad (5)$$

For GRT this becomes a critical distinction: the importance functions needed to guide a random walk towards zero-variance satisfy the integral equation for collision density

$$C(\mathbf{x}, \omega) = \int_0^\infty p_c(s) \int_{4\pi} \alpha P(\omega' \rightarrow \omega) C(\mathbf{x} - s\omega, \omega') d\omega' ds. \quad (6)$$

The adjoint incoming radiance field in the scene [Novák et al. 2018] is of little use for path guiding.

## 6.4 Guiding-to-Escape in a Half Space

We turn now to a half space escape problem that will form the basis for much of the following sections. We assume a homogeneous semi-infinite 3D medium defined by  $x > 0$  with a flat indexed-matched boundary and isotropic scattering and absorption in the interior (see Figure 4).

### 6.4.1 Sources and Detectors

A linear transport problem is defined by specifying a medium/scene, its properties and boundaries, and a set of light sources. We then define a detector sensitivity or measurement functional over the phase space (typically just a camera in rendering). In the general case, we seek a zero variance estimator that has particles leaving the sources and arriving at the detectors such that every simulated particle reaches a detector and reaches it such that the particle weight times the detector sensitivity at that position and direction is a constant. In this general case, the first step of the zero variance derivation is to determine the guided spatial and angular distributions from which to leave the sources [Hoogenboom 2008a]. In the case of BSSRDF sampling, however, our source is always a single element of phase space: an incident position and direction, which we always sample with weight  $w = 1$ . Since we assume a flat homogeneous geometry, it suffices to only know the incident cosine, and so we will derive 1D families of estimators over  $\mu_i$ . Our detector sensitivity is defined as 1 for all positions and directions that escape the medium.

### 6.4.2 The Classical Estimator

We are given as a starting point that a particle arrives at the boundary entering the medium along a direction with a cosine to the inward normal of  $\mu_i$ . The classical estimator proceeds with (see Figure 4)

1. Particle weight  $w = 1$
2. Sample initial displacement  $s_1$  from  $p_u(s)$  and move particle
3. Absorb  $w \rightarrow w * \alpha$

4. Sample direction  $\omega$  from phase function  $P$
5. Sample intercollision displacement  $s$  from  $p_c(s)$  and move particle
6. if  $x < 0$  return/score  $w$  at the exitant boundary position and direction and terminate the walk
7. goto 3.

### 6.4.3 The Guided Estimator

The key shortcoming of the classical estimator is that the sampling of  $p_u(s)$ ,  $P$  and  $p_c(s)$  are locally greedy—they are perfect estimators of these normalized distributions, but are ignorant of the end goal, like playing chess while only thinking one move ahead. We will derive the zero variance estimator for escaping the half space by guiding each of these three sampling decisions. The distributions that are required to achieve zero variance depend on the position and direction of the particle right before these sampling steps are performed and are uniquely determined from a value or importance function  $W$  that satisfies an adjoint integral transport equation for collision rate density inside the volume [Hoogenboom 2008a]. In the final step we will also adjust the escape scoring to use an expected value estimator.

**Initial Free Flight:** Our first step is to sample the initial free-flight distance  $s_1$  from a guided distribution  $p_1(s)$  that achieves the zero-variance goal. In sampling  $s_1$  from  $p_1(s)$  instead of  $p_u(s)$ , the particle must adopt a weight factor of  $w_1(s_1) = p_u(s_1)/p_1(s_1)$ . After traversing free-flight distance  $s_1$  the particle enters a collision at depth  $x_1 = \mu_i s_1$  with weight  $w_1(s_1)$ . Let  $W(x, \mu)$  be the probability that a particle entering a collision at depth  $x$  along direction with cosine  $\mu$  eventually escapes the medium. The expected contribution of our particle after initial displacement is therefore its current state times the expected total future state,  $w_1(s_1)W(x_1, \mu_i)$ . For the random walk to be zero variance this result must be a constant, and that constant must be equal to the diffuse albedo of the medium for incoming direction  $\mu_i$

$$w_1(s_1)W(x_1, \mu_i) = \frac{p_u(s_1)}{p_1(s_1)} W(\mu_i s_1, \mu_i) = R(\mu_i). \quad (7)$$

From this we see that  $p_1(x)$  must be

$$p_1(s) = \frac{p_u(s)W(s\mu_i, \mu_i)}{R(\mu_i)}. \quad (8)$$

We see that the guided distribution is the product of the analog distribution and the importance function with a normalization factor. We don't need to know  $R(\mu_i)$ , because we can find it by simply requiring that  $p_1(s)$  integrates to 1. For no absorption, we see  $R = 1$ ,  $W(x) = 1$  and analog sampling  $p_1(s) = p_u(s)$ , as desired.

**The Full Guided Estimator:** The previous example illustrates the key components of the general procedure for deriving each step of a random walk in order to achieve zero variance:

- The end state of a guided step will be the resulting particle weight and the particle position and direction
- The resulting particle weight will be the prior weight times the ratio of the analog and guided distributions at the sampled distance/direction
- There is a unique probability to escape the medium at the sampled particle position and direction (importance  $W$ ). Care must be taken here to distinguish between entering and leaving collisions.
- The guided distribution must be the normalization of  $W$  times the analog distribution.

We will see the details of the remaining steps in the general procedure during the following examples.

To summarize the notation (also summarized in Table 1) of the upcoming guided distributions: absorption is handled identically to the classical random walk, applying implicit capture per collision with

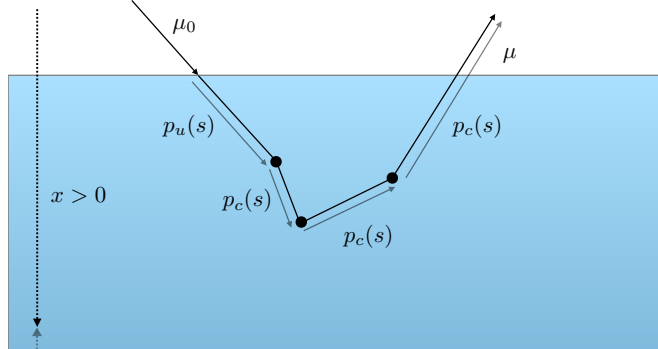


**Figure 4:** For guided BSSRDF sampling we consider the illustrated GRT random walk in a 3D half space. A particle arriving along a direction with cosine  $\mu_0$  enters the medium and collides after a distance drawn from  $p_u(s)$ . Absorption with probability  $1 - \alpha$  occurs at each collision event. If not absorbed, the particle continues after phase function sampling until exit is sampled. Each zero-variance derivation assumes some importance function for escape  $W(x)$  when entering collision at depth  $x$  and from this follows guided distributions  $p_1(s)$  for the initial free-path lengths and related distributions for direction and intercollision length sampling. These distributions and their related weight adjustments are summarized in Table 1.

weight factor  $\alpha$ . Phase function sampling requires polar  $\mu$  and azimuthal  $\phi$  angle decisions drawn from guided distributions  $P^g(\mu; x)$  and a uniform azimuth distribution  $1/2\pi$ , respectively. The guided azimuthal sampling is identical to the analog case because of the plane symmetry of the medium and detector sensitivity, so the weight factor for azimuthal guiding is  $w_\phi = (1/2\pi)/(1/2\pi) = 1$ . For polar angle sampling,  $w_\mu = (1/2)/P^g(\mu; x)$  accounts for guiding away from the uniform (1/2) distribution of isotropic scattering. Weight factor  $w_s = p_c(s)/p_c^g(s; x, \mu)$  accounts for the guided intercollision free-path length sampling from  $p_c^g(s; x, \mu)$ .

## 6.5 Two Exactly-Zero-Variance Walks

Achieving a perfectly zero-variance walk for a given problem is almost always more challenging than estimating the desired quantity, because the importance function is required everywhere in the scene. However, it can still be useful to apply the theory using an approximate importance  $W(x)$ , to reduce the absorption variance. This can improve upon classical sampling even if the geometry is curved, if the medium coefficients vary with position or if there is other geometry imbedded in the medium. Since there are several examples with isotropic scattering in half spaces where the exactly zero variance estimator is possible, we will review those in order to best demonstrate how zero variance walks are derived and how they differ from the classical estimators.

The first example we consider is for the reflection from a classical half rod with isotropic scattering: a simplified one-dimensional domain where particles can only move in one of two discrete directions, left (-) and right (+). Because the collision rate density in the half rod is a simple exponential, the guiding importance sampling decisions can be handled analytically and we avoid the complexity of the singular eigenfunctions of the related problem in a 3D half space.

Sampling Decision	Analog	Guided	Weight Factor
Initial free-path length $s_1$ from the boundary	$p_u(s)$	$p_1(s)$	$w_1 = \frac{p_u(s_1)}{p_1(s_1)}$
Intercollision free-path length $s$	$p_c(s)$	$p_c^g(s; x, \mu)$	$w_s = \frac{p_c(s)}{p_c^g(s; x, \mu)}$
Direction cosine $\mu$	(1/2)	$P^g(\mu; x)$	$w_\mu = \frac{(1/2)}{P^g(\mu; x)}$
Direction azimuth $\phi$	(1/2π)	(1/2π)	$w_\phi = \frac{(1/2\pi)}{(1/2\pi)} = 1$

**Table 1:** Summary of our notation for the analog and guided distributions for planar guiding to escape in a homogeneous GRT volume.

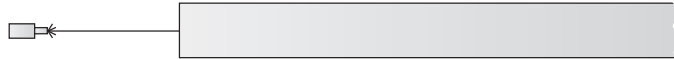


**Figure 5:** The Albedo problem for the half rod.

The second example we consider is a new derivation for GRT in a 3D half space where free-path lengths between collision are drawn from a Gamma/Erlang-2 distribution. This zero variance estimator shows how the zero-variance theory extends to easily handle GRT. We will also see that a projection of this random walk onto the depth axis is equivalent to our first example in the rod.

### 6.5.1 The Zero-Variance Walk in the Half Rod: Křivánek's Walk

We now consider the problem of external illumination reflecting from a one-dimensional absorbing and scattering half space with isotropic scattering and vacuum boundary conditions (Figure 5). We consider specifically the *rod model*<sup>2</sup>—a simplified one-dimensional domain in which particles can only flow right or left ([Wing 1962; Hoogenboom 2008b]). This problem corresponds to the classical albedo problem of linear transport theory [Chandrasekhar 1960], but in a 1D universe—the unique dimensionality for which the full solution both at the boundary and internally is known exactly in terms of simple explicit expressions [d'Eon and McCormick 2019].

While 1D rod transport has limited direct physical application [Zoia et al. 2011], study of this problem provides all of the essential ingredients for building a zero-variance half space walk, without the distraction of complex importance functions. The rod has been used several times to demonstrate zero-variance walks [Hoogenboom 1981; Hoogenboom 2008b]. However, to our knowledge, the zero variance walk we derive in this section is new<sup>3</sup>.

Let us define the half rod to occupy the positive axis  $x > 0$  with direction  $\omega = 1$  corresponding to flight deeper into the rod and  $\omega = -1$  towards the boundary. The phase space for monoenergetic particles/photon is then  $\mathbb{R} \times \{-1, 1\}$ . Scattering is isotropic, where each collision draws a new direction  $\omega$  from  $\{-1, 1\}$  with equal probability, and the single-scattering albedo is  $\alpha$ . This example assumes classical media with exponential free-path length distributions and attenuation laws  $p_c(s) = p_u(s) = X_c(s) = e^{-s}$ .

Our random walk begins entering the rod at the boundary  $x = 0, \omega = 1$  and proceeds with an initial free-flight transition followed by a chain of collision and free-flight steps until the particle is either absorbed or escapes. The analog walk chooses between collision and absorption with a discrete binary decision and clearly leads to unresolvable variance, so the first step in guided sampling is to use implicit

<sup>2</sup>Also known as the two-directional or Fermi model

<sup>3</sup>This result was communicated to the first author by the second author on Nov 24, 2013 and has been named to reflect its origin.

capture, as is standard in volumetric light transport. This is accounted for by a particle weight  $w$  that begins the walk at 1 and is multiplied by the single-scattering albedo for every collision inside the rod.

Next, following Hoogenboom [2008a], we extend the rod to the full line, letting the exterior portion  $x < 0$  be purely absorbing. This is a mathematical convenience that informs derivation of the importance function for the entire system that is used to guide the random walk. In this extended interpretation of the problem, any collision in  $x < 0$  scores the current particle weight and terminates the walk. Any absorption inside the rod scores 0 and continues. This imparts a *last event collision estimator* interpretation on escaping the medium.

We now define an importance (or value) function  $W(x, \omega)$  for the rod defined as follows:  $W(x, \omega)$  is the probability that a particle *entering* a collision at position  $x$  moving in direction  $\omega$  (before the collision) eventually escapes the rod. From the assumption of isotropic scattering we see immediately that the desired importance function is independent of direction  $\omega$ . This is a hallmark of deriving zero variance walks for problems with isotropic scattering: the dimensionality of the importance function is greatly reduced.

We can find  $W(x)$  from known solutions for the collision rate density inside a half rod due to external illumination. The two are directly related, by reciprocity. The specific solution follows from solving a Wiener-Hopf integral equation with the Picard/Lalesco kernel[Wing 1962; d'Eon and McCormick 2019] (more on this later). The result is

$$W(x) = \begin{cases} (1 - \sqrt{1 - \alpha}) e^{-\sqrt{1 - \alpha}x}, & x \geq 0 \\ 1 & x < 0 \end{cases} \quad (9)$$

where we have set the value to 1 for any position outside of the volume.

We note several important features of this result. For the conservative medium  $\alpha = 1$ ,  $W(x) = 1$  everywhere because entering a collision anywhere eventually leads to escape, which shows that the classical random walk estimation of the albedo  $R$  is already zero variance. Given  $W$ , we immediately have the final weight of our zero-variance walk, the escape probability, given by

$$R = \int_0^\infty p_u(s)W(s)ds = \int_0^\infty e^{-s}W(s)ds = \frac{2}{\alpha} (1 - \sqrt{1 - \alpha}) - 1. \quad (10)$$

**Initial Free Flight:** Following the arguments from the previous section we see that  $p_1(x)$  must be

$$p_1(x) = \frac{p_u(x)W(x)}{R}. \quad (11)$$

We find that  $p_1(x)$  simplifies to a simple exponential

$$p_1(x) = (\sqrt{1 - \alpha} + 1) e^{-(\sqrt{1 - \alpha} + 1)x}, \quad (12)$$

which we can easily importance sample by CDF inversion, giving

$$x_1 = -\frac{\log(1 - \xi)}{1 + \sqrt{1 - \alpha}} \quad (13)$$

where  $\xi \in [0, 1]$  is a uniform random variate.

**Direction Sampling:** For each collision at depth  $x > 0$  we need to sample an outgoing scattering direction  $\omega$  such that the future contributions from subsequent collision and escape are perfectly balanced.

Let the guided distribution  $p^+(x)$  be the probability that the positive direction is sampled after collision at depth  $x$ , and  $p^-(x) = 1 - p^+(x)$  the probability of scattering towards the boundary. This is a discrete variant of  $P^g(\mu; x)$  described in the previous section. For every collision, the particle enters with weight  $w = R/W(x)$ . Immediately following the collision the weight is adjusted by implicit capture to  $w' = \alpha R/W(x)$ . If the particle scatters positive, we have a further weight adjustment of  $w_\omega = (1/2)/p^+(x)$  due to guiding away from the analog choice of equal probabilities for both directions. The expected score of the particle having gone right is then the total weight after scattering,  $w'w_\omega$ , multiplied by the expected final score over all possible free-flight distances  $s$ ,

$$w'w_\omega \int_0^\infty p_c(s)W(x+s)ds = R \quad (14)$$

Solving this equation for  $p^+(x)$  we find simply

$$p^+(x) = \frac{1}{2}(1 - \sqrt{1 - \alpha}). \quad (15)$$

Remarkably, this result is invariant to depth—no matter where we collide in the rod, we need to sample away from the boundary with the same probability that depends only on the absorption level in the rod. As absorption increases and  $\alpha$  decreases, we sample towards the boundary with increasing probability—paths are guided towards the exit. When there is no absorption ( $\alpha = 1$ ) we recover the analog phase function sampling  $p^+(x) = (1/2)$ , as desired.

Direction  $\omega$  is easily sampled from  $\{p^+(x), p^-(x)\}$  using a single random number for the discrete choice. The weight factor due to this importance sampling simplifies to

$$w_\omega = \begin{cases} \frac{1}{1+\sqrt{1-\alpha}}, & \omega = -1 \\ \frac{1}{1-\sqrt{1-\alpha}}, & \omega = 1 \end{cases}. \quad (16)$$

**General Free-Path Sampling:** The final step in building the zero-variance walk for the rod is to determine the guided intercollision free-path length distribution  $p_c^g(s; x, \omega)$  and to handle the case where the particle exits the volume. Here,  $p_c^g(s; x, \omega)ds$  is the probability that we sample a guided distance-to-collision  $s$  falling in  $[s, s + ds]$  when leaving a collision at  $x$  in direction  $\omega$ .

In the case of moving in the positive direction,  $\omega = 1$ , we need to sample a intercollision distance  $s^+$  from a distribution proportional to  $p_c(s)W(x+s)$ . This results in the same exponential distribution we saw above for the initial collision depth  $x_1$  and so we have

$$p_c^g(s; x, 1) = p_1(s) \quad (17)$$

with sampling procedure given in Eq.(13). For free-flight distances  $s$  in the negative direction we again need to sample from the normalized distribution that is proportional to the product of  $p_c(s)$  and the importance function  $p_c(s)W(x-s)$ . We find the normalization constant to be

$$\int_0^\infty p_c(s)W(x-s)ds = e^{\sqrt{1-\alpha}(-x)}, \quad (18)$$

resulting in

$$p_c^g(s; x, -1) = (1 - \sqrt{1 - \alpha}) \left( e^{-s(1 - \sqrt{1 - \alpha})} \right), \quad 0 < s < x. \quad (19)$$

Like the positive direction case, we again find a distribution that is translationally invariant. The shape of the PDF beyond the boundary  $s > x$  is not important—we only need to observe that this distribution up

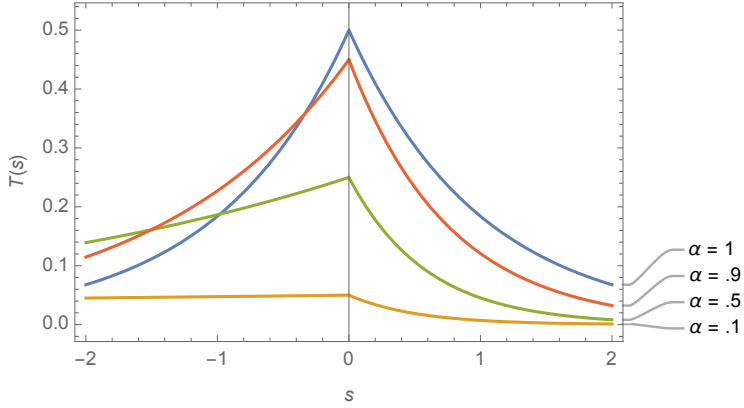


**Figure 6:** Guided transition kernels  $T(s)$  (combining phase function and free-flight sampling) for the zero-variance walk in the half rod. With decreasing single-scattering albedo  $\alpha$  negative displacements towards the boundary (escape) are increasingly preferred.

to the boundary is an exponential with a mean free path of  $1/(1 - \sqrt{1 - \alpha})$  and sample that distribution. Any time a distance past the boundary is sampled, we apply a mean-value weight factor  $w_{\text{esc}}$ , which is the ratio of the analog probability for escape to the probably of escaping with the guided distribution

$$w_{\text{esc}} = \frac{X_c(x)}{e^{-x(1-\sqrt{1-\alpha})}}. \quad (20)$$

Finally, if we sample an interior collision  $s < x$ , we apply the weight factor for the guided free-path length

$$w \rightarrow w * \frac{p_c(s)}{p_c^g(s; x, -1)}. \quad (21)$$

This completes the derivation of the zero-variance walk. We include a Mathematica implementation of it in the supplemental material.

It is informative to look at combined transition kernel  $T(s)$  that combines direction and displacement sampling together using a signed free-flight distance  $s$  where the sign indicates whether or not the depth of the next collision is closer to the boundary and farther into the rod. We find

$$T(s) = \begin{cases} \frac{\alpha}{2} e^{s(1-\sqrt{1-\alpha})}, & s < 0 \\ \frac{\alpha}{2} e^{-s(1+\sqrt{1-\alpha})}, & s > 0 \end{cases}. \quad (22)$$

These guided displacement kernels are plotted in Figure 6 for various absorption levels and show how increased absorption leads to increased preference for negative (towards the boundary) displacements in order to get the particle out before it is overly absorbed. Figure 7 shows the relative change in particle weight after a net positive or negative displacement in the rod with the zero-variance scheme. It is interesting that this shows no discontinuity at 0 displacement.

### 6.5.2 The Zero-Variance Walk in the Gamma-2 Half Space

In this section we derive the first perfectly-zero-variance walk for escaping an absorbing half space in 3D. To our knowledge, this is also the first zero-variance walk of any form derived for GRT.

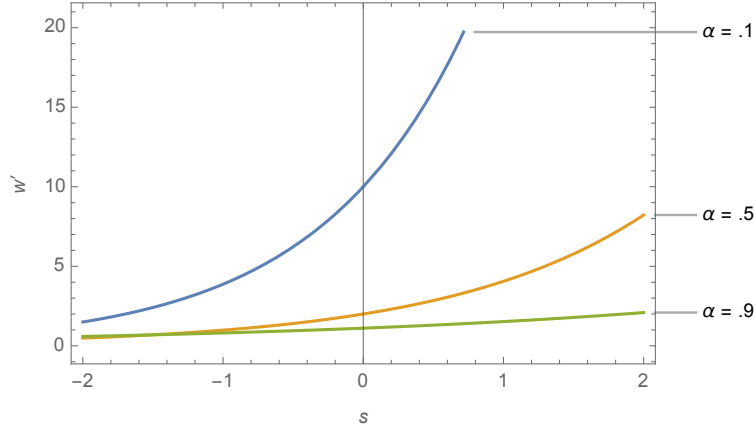


**Figure 7:** Relative change in particle weight  $w'$  in transitioning a relative distance  $s$  in the rod.

Specifically, we consider the 3D half space  $x > 0$  with Gamma-2-distributed free-path lengths between collisions. Upon specifying  $p_c(s)$ , the following full set of GRT statistics follow [d'Eon 2018]

$$p_c(s) = e^{-s}s, \quad (23)$$

$$X_c(s) = e^{-s}(1+s), \quad (24)$$

$$p_u(s) = \frac{e^{-s}(1+s)}{2}. \quad (25)$$

**Importance:** As in any zero or near-zero variance random walk derivation, we begin with the importance function, which in the present case is the probability to eventually escape the medium (after any number of subsequent collisions) upon entering a collision at depth  $x$ . Because the scattering is isotropic, the importance function  $W(x)$  is independent of the incoming direction of the particle.

We can derive or estimate  $W(x)$  in a number of ways. We could tabulate a discrete numerical approximation of  $W(x)$  for a given absorption level by taking the mean escape probability of some number of unguided random walks, each beginning in some narrow interval of depths  $x_0 \in [x, x + dx]$ . Alternatively, by reciprocity, we could sample a suitably weighted uniform surface source and tally collision densities in narrow depth intervals within the medium. We have chosen a problem which admits an exact and very simple importance function in order to clearly illustrate the subsequent steps in determining the full guided walk. However, all of the following principles apply to any approximate tabulated or fitted function  $W(x)$ .

We now derive the exact escape probability for our problem from the Wiener-Hopf integral equation that applies to the collision rate density inside the volume. The details of this derivation are not essential to the guiding sampling that follows, but we include these details for completeness. The Wiener-Hopf integral equation for the collision rate density  $C(x)$  with a unit Dirac delta of initial collisions at depth  $x_0$  is

$$C(x) = \delta(x - x_0) + \alpha \int_0^\infty C(x') K_C(x - x') dx'. \quad (26)$$

The displacement kernel  $K_C$  for Gamma-2 flights in 3D with isotropic scattering follows from [d'Eon

and McCormick 2019; d’Eon 2019b]

$$K_C(x) = \frac{1}{2} \int_0^1 p_c(|x|/\mu) \frac{1}{\mu} d\mu = \frac{1}{2} e^{-|x|}, \quad (27)$$

which is the Picard/Lalesco kernel [Picard 1911]. From the Fourier transform of the kernel

$$\tilde{K}_C(t) \equiv \int_{-\infty}^{\infty} K_C(x) e^{ixt} dx = \frac{1}{1+t^2} \quad (28)$$

we immediately have the Green’s function (the solution to Eq.(26)) in terms of the Chandrasekhar  $H$  function for the problem. In general,  $H$  is given uniquely by [Ivanov 1994]

$$H(z) = \exp \left( \frac{z}{\pi} \int_0^{\infty} \frac{1}{1+z^2 t^2} \log \left[ \frac{1}{1-\alpha \tilde{K}_C(t)} \right] dt \right), \quad \operatorname{Re} z > 0. \quad (29)$$

For the Picard kernel we find [d’Eon and McCormick 2019]

$$H(\mu) = \frac{(1+\mu)}{(1+\mu/\nu_0)} \quad (30)$$

where  $\nu_0$  is the discrete eigenvalue of the transport operator, the unique positive solution of the dispersion equation,

$$1 - \alpha \tilde{K}_C(i/\nu_0) = 0, \quad \nu_0 = \frac{1}{\sqrt{1-\alpha}}. \quad (31)$$

If we define the Laplace transform

$$\mathcal{L}_x[f(x)](s) \equiv \int_0^{\infty} f(x) e^{-sx} dx, \quad (32)$$

then we have, from Ivanov ([1994], Eqs. (19) and (21)), that the double Laplace transform of the Green’s function is

$$\bar{\mathbb{G}}(s, s_0) = \mathcal{L}_x[\mathcal{L}_{x_0}[\mathbb{G}(x, x_0)]](s, s_0) = \frac{H(1/s)H(1/s_0)}{s+s_0}. \quad (33)$$

Inverting both Laplace transforms gives the Green’s function  $\mathbb{G}(x, x_0)$ , which is the rate density of collisions in the system at  $x$  due to the initial collision at depth  $x_0$ . However, we only need to invert one of the Laplace transforms, because we want the total rate of collisions inside the entire half space, which is conveniently given when  $s = 0$  in Eq.(33). To find the total collision rate  $\langle C(x_0) \rangle$ , we therefore take the inverse Laplace transform of  $\bar{\mathbb{G}}(0, s_0)$  with respect to  $s_0$ ,

$$\begin{aligned} \langle C(x_0) \rangle &= \mathcal{L}_{s_0}^{-1} \left[ \frac{H(\infty)H(1/s_0)}{s_0} \right] (x_0) = \mathcal{L}_{s_0}^{-1} \left[ \frac{(1+s_0)\nu_0^2}{s_0(s_0\nu_0+1)} \right] (x_0) \\ &= \nu_0 \left( \nu_0 - (\nu_0 - 1)e^{-\frac{x_0}{\nu_0}} \right) \end{aligned} \quad (34)$$

where here we have used  $H(\infty) = 1/\sqrt{1-\alpha}$  [Ivanov 1994]. The mean absorption per collision is  $1-\alpha$ , and there are a mean number of collisions given by  $\langle C(x_0) \rangle$ , and so the mean energy not absorbed in the system is (and by normalization, the escape probability) is  $1 - (1-\alpha)\langle C(x_0) \rangle$ , giving our importance function for the problem,

$$W(x) = \begin{cases} \frac{(\nu_0-1)e^{-\frac{x}{\nu_0}}}{\nu_0}, & x \geq 0 \\ 1 & x < 0 \end{cases} \quad (35)$$

Eq.(35) is, in fact, the exact same importance function for the exponential half rod example above (Eq.(9)).

The last quantity we need for deriving the zero variance walk is the expected value of our estimator for a single particle arriving at the boundary along cosine  $0 < \mu_i \leq 1$  to the  $x$  axis. The known albedo for the problem is [d'Eon 2019b]

$$R(\alpha, \mu_i) = \int_0^\infty p_u(s)W(s\mu_i)ds = \frac{\alpha(\sqrt{1-\alpha}\mu_i + 2)}{2(\sqrt{1-\alpha} + 1)(\sqrt{1-\alpha}\mu_i + 1)^2}. \quad (36)$$

**Initial Free-Flight Distance:** Guided sampling of the initial free-flight distance  $s_1$  is found from normalizing the product of the uncorrelated-origin FPD and the importance function at depth  $\mu_i s$  yielding

$$p_1(s, \mu_i) = \frac{p_u(s)W(\mu_i s)}{R(\alpha, \mu_i)} = e^{-s\left(\frac{\mu_i}{\nu_0} + 1\right)}(s+1)\frac{\left(\frac{\mu_i}{\nu_0} + 1\right)^2}{\frac{\mu_i}{\nu_0} + 2} \quad (37)$$

Using three independent uniform random variates  $\xi_1, \xi_2, \xi_3$ , we can sample this as a sum of an exponential and an Erlang-2 distribution,

$$s_1 = \begin{cases} -m(\mu_i) \log(\xi_2), & \xi_1 < \frac{1}{1+m(\mu_i)} \\ -m(\mu_i) \log(\xi_2 \xi_3), & \text{else} \end{cases} \quad (38)$$

where

$$m(\mu) = \frac{1}{1 + \frac{\mu}{\nu_0}} \quad (39)$$

is a path-length stretching factor.

**Guided Direction Sampling:** Let us define the new angular importance function

$$W_o(x, \mu) = \int_0^\infty W(x + \mu s)p_c(s)ds \quad (40)$$

for *leaving* a collision. This function takes the analog probability  $p_c(s)ds$  that the next collision is within  $ds$  of  $s$  away from the starting position, and multiplies by the probability  $W(x + \mu s)$  of escaping after collision there. Integration over all possible  $s$  then gives the mean probability of eventually escaping the medium when leaving a collision at depth  $x$  in direction  $\mu$ . Zero-variance direction sampling then results from drawing outgoing direction cosines  $\mu$  from the normalization of  $P(\mu)W_o(x, \mu)$ . This is the same general form we saw when deriving the initial path length but note here the different importance function  $W_o$ . It is essential that each step in the zero variance derivation carefully consider the escape probability immediately following the action that is being sampled, and to distinguish between pre/post absorption and collision, or for hitting or leaving a Fresnel boundary, etc.

The analog direction cosine phase function is isotropic  $P(\mu) = (1/2)$ . We seek a guided direction distribution  $P^g(\mu; x) = aP(\mu)W_o(x, \mu)$  where constant  $a$  is chosen to achieve normalization

$$\int_{-1}^1 P^g(\mu; x)d\mu. \quad (41)$$

After some calculations in Mathematica, we find

$$P^g(\mu; x) = \begin{cases} \frac{\frac{v^2-1}{2(\mu+\nu_0)^2},}{(\nu_0+1)\left(e^{z\left(\frac{1}{\mu}+\frac{1}{\nu_0}\right)}\left(\mu\left(\mu^2+2\mu\nu_0+\nu_0\right)-(\mu+1)z(\mu+\nu_0)\right)+\mu(\nu_0-1)\nu_0\right)}, & \mu > 0 \\ \frac{2\mu\nu_0(\mu+\nu_0)^2}{2\mu\nu_0(\mu+\nu_0)^2}, & \mu < 0. \end{cases}$$

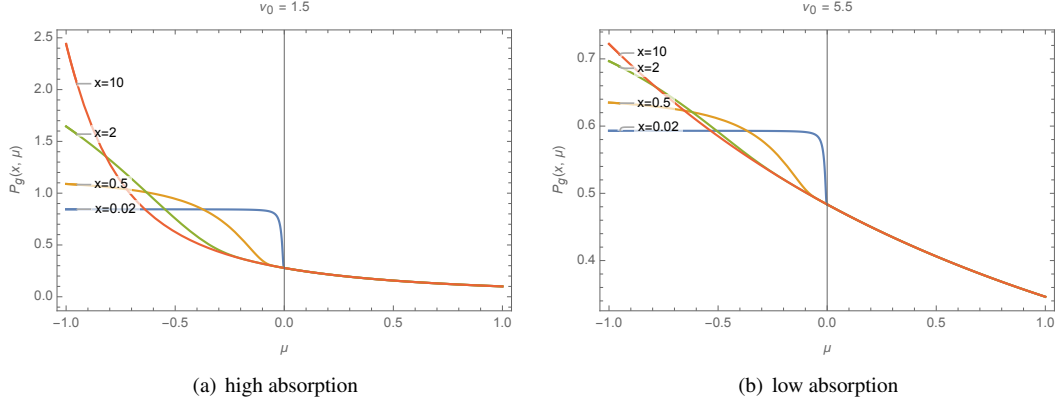


**Figure 8:** The zero-variance walk in 3D with Gamma-2 flights samples upwelling  $\mu < 0$  collisions more often than downwelling ones. Nearer the boundary the upwelling distribution flattens into a uniform distribution because all directions lead to escape with negligible attenuation. The downwelling direction sampling is independent of depth  $x$ .

Remarkably, the angle selection in the downward hemisphere (away from the boundary  $\mu > 0$ ) does not depend on the depth  $x$  of the particle. This is because the importance function is a pure exponential. Gamma-2 random flights are the unique distribution  $p_c(s)$  that produce this result in 3D under isotropic scattering.

To sample this distribution over outgoing cosine  $\mu \in [-1, 1]$  we split the sampling into the downwelling (+) and upwelling (-) hemispheres. Because the downwelling direction sampling is independent of depth, the total probability of choosing a downwelling direction must too be depth-independent and, indeed, we find

$$p^+ \equiv \int_0^1 P^g(\mu; x) d\mu = \frac{1}{2} (1 - \sqrt{1 - \alpha}) . \quad (42)$$

Choosing a downwelling direction with probability  $p^+$  we need to sample a direction cosine  $\mu$  from

$$\frac{P^g(\mu; x)}{p^+} = \frac{\nu_0(\nu_0 + 1)}{(\mu + \nu_0)^2}, \quad 0 < \mu < 1. \quad (43)$$

From CDF inversion we find a downwelling cosine  $\mu^+$  is sampled using

$$\mu^+ = \frac{\nu_0 + \xi}{1 + \nu_0 + \xi} \quad (44)$$

where  $0 < \xi < 1$  is a uniform random variate.

Sampling upwelling direction cosines is more challenging. We need to sample from

$$\frac{P^g(\mu; x)}{1 - p^+} = \frac{\mu(\nu_0 - 1)\nu_0 + e^{x\left(\frac{1}{\mu} + \frac{1}{\nu_0}\right)} \left(\mu(\mu^2 + 2\mu\nu_0 + \nu_0) - (\mu + 1)x(\mu + \nu_0)\right)}{\mu(\mu + \nu_0)^2}$$

with CDF

$$\int_{-1}^k \frac{P^g(\mu; x)}{1 - p^+} d\mu = \frac{(k+1) \left( k e^{x \left( \frac{1}{k} + \frac{1}{\nu_0} \right)} + \nu_0 \right)}{k + \nu_0}, \quad -1 < k < 0. \quad (45)$$

We did not find an exact sampling procedure for this distribution but found 3 iterations of Newton's method started at  $\mu = -0.5$  very accurate for the limited testing we undertook.

**General Free-Flight Sampling:** For downwelling directions we find a simple guided free-path length distribution by normalizing  $p_c(s)W(x + s\mu)$ , similar to the initial free-path length procedure above, but with  $p_c(s)$  instead of  $p_u(s)$  because the particle is leaving a collision and not a deterministic location on the boundary. We find,

$$p_c^g(s; x, \mu) = \frac{se^{-\frac{s}{m(\mu)}}}{m(\mu)^2}, \quad 0 < \mu < 1, \quad (46)$$

which is a stretched Gamma-2 distribution with factor  $m$  given in Eq.(39) that is easily importance sampled via

$$s^+ = -m(\mu) \log(\xi_1 \xi_2). \quad (47)$$

Note how similar this is to Asymptotic/Dwivedi guiding in the classical 3D half space. This is a direct generalization of the exponential transform that was the original guiding tool of choice in neutron transport literature [Dwivedi 1982]. Here, we find an analogous stretching of the intercollision free-path distribution, the Gamma-2 transform, appearing in the exactly-zero-variance walk.

For the upwelling directions, we again find the guided free-path length distribution by normalizing  $p_c(s)W(x + s\mu)$ , but find

$$\begin{aligned} & \int_0^\infty p_c(s)W(x + s\mu)ds \\ &= \frac{e^{-\frac{x}{\nu_0}} \left( \mu(\nu_0 - 1)\nu_0 + e^{x\left(\frac{1}{\mu} + \frac{1}{\nu_0}\right)} (\mu(\mu^2 + 2\mu\nu_0 + \nu_0) - (\mu + 1)x(\mu + \nu_0)) \right)}{\mu(\mu + \nu_0)^2} \end{aligned}$$

Past  $s = -x/\mu$  we will escape the boundary, so we only need to compute this probability and sample a continuous depth in the case that we do not escape. We find the escape probability

$$\begin{aligned} p_{esc}(x, \mu) &= \frac{\int_{-x/\mu}^\infty p_c(s)W(x + s\mu)ds}{\int_0^\infty p_c(s)W(x + s\mu)ds} \\ &= \frac{(\mu + \nu_0)^2(\mu - x)e^{x\left(\frac{1}{\mu} + \frac{1}{\nu_0}\right)}}{\mu(\nu_0 - 1)\nu_0 + e^{x\left(\frac{1}{\mu} + \frac{1}{\nu_0}\right)} (\mu(\mu^2 + 2\mu\nu_0 + \nu_0) - (\mu + 1)x(\mu + \nu_0))}. \quad (48) \end{aligned}$$

If we sample to stay inside the medium, using a random choice  $\xi > p_{esc}(x, \mu)$  then we sample a free-path length distance  $s$  from

$$\begin{aligned} p_c^g(s; x, \mu) &= \frac{p_c(s)W(x + s\mu)}{\int_0^\infty p_c(s)W(x + s\mu)ds} \\ &= -\frac{\mu s (\mu + \nu_0)^2 e^{-\frac{s(\mu + \nu_0)}{\nu_0}}}{\nu_0 \left( e^{x\left(\frac{1}{\mu} + \frac{1}{\nu_0}\right)} (\mu\nu_0 - x(\mu + \nu_0)) - \mu\nu_0 \right)}, \quad -1 < \mu < 0. \quad (49) \end{aligned}$$

We can sample this by CDF inversion finding

$$s = \frac{\nu_0 \left( -W_{-1} \left( \xi \left( e^{x\left(\frac{1}{\mu} + \frac{1}{\nu_0}\right)} - 1 \left( x \left( \frac{1}{\mu} + \frac{1}{\nu_0} \right) - 1 \right) + \frac{1}{e} \right) - \frac{1}{e} \right) \right) - \nu_0}{\mu + \nu_0} \quad (50)$$

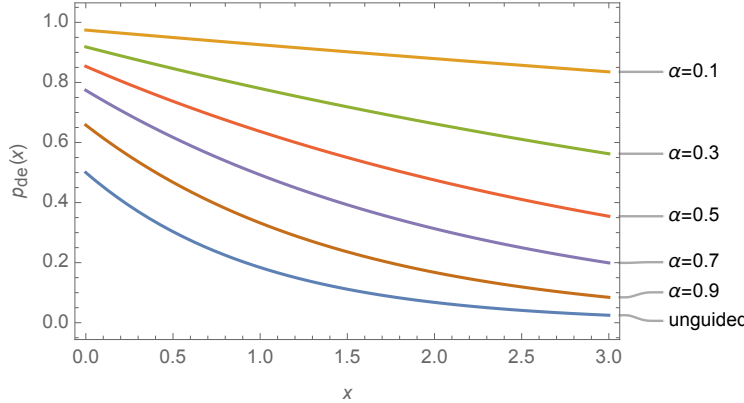


**Figure 9:** The probability of directly escaping the medium with no further collisions  $p_{de}(x)$  when leaving a collision at a depth  $x$  in the half space. The guided walk prefers direct escape with increasing probability as the single-scattering albedo  $\alpha$  reduces. For the classical unguided/analog walk, the direct escape probability is independent of  $\alpha$  and equal to  $1/2$  at the boundary  $x = 0$ .

where  $W_{-1}(x)$  is a Product Log function.

If an escape is sampled, we incur one last weight factor using an expected value optimization, the ratio of the analog escape probability to the corresponding guiding escape probability. From depth  $x$  along direction  $-1 < \mu < 0$  we escape along the final path length of  $d = -x/\mu$ . The analog escape probability leaving a correlated event (the last collision) is then  $X_c(d)$ . The weight factor for escape is thus

$$w_{esc} = \frac{X_c(d)}{p_{esc}(x, \mu)}. \quad (51)$$

This completes the derivation of the zero variance walk, and illustrates all of the essential steps in deriving an exact or near-zero-variance walk for escape a 3D half space with no Fresnel interactions at the bounadry.

**Translationally-Invariant Guiding with Exit Resampling:** Our derivation above has taken a purely sequential approach for determining the guided walk: a complete free-path-length distribution is determined and sampled, and then a phase function distribution, and back and forth until escape. This has led to rather complicated distributions in the upwelling hemisphere due to the discontinuity in the importance function past the boundary. It turns out that many of these complexities can be avoided if we instead sample directions and displacements assuming a non-truncated exponential importance that now extends upward past 1 outside of the volume,

$$W(x) = e^{-x/\nu_0}. \quad (52)$$

Regardless of initial depth, the guided displacement and direction sampling steps using this importance function reduce to the downwelling equations above but for all directions  $-1 < \mu < 1$ . The angular distribution that we sample over the full sphere is now the generalized discrete Case eigenfunction for our Gamma-2 flight [d'Eon 2019b]

$$\phi(\mu, \nu_0) = \frac{c}{2} \left( \frac{1}{1 + \mu/\nu_0} \right)^2. \quad (53)$$

With CDF inversion we find sampling of outgoing polar angle  $\mu$  from

$$-\frac{-2\nu_0\xi + \nu_0 + 1}{\nu_0 - 2\xi + 1}, \quad (54)$$

where  $\xi \in [0, 1]$  is a uniform random variate. Given outgoing  $\mu$ , displacement sampling follows from Eq.(46) for all  $-1 < \mu < 1$ . The probability that this procedure escapes the volume over all possible outgoing directions is (using Eq.(48))

$$p_{esc\phi}(x) = \int_{-1}^0 \phi(\mu, \nu_0) p_{esc}(x, \mu) d\mu = \frac{(\nu_0 + 1) e^{(\frac{1}{\nu_0} - 1)x}}{2\nu_0} \quad (55)$$

and it can be shown that this exactly matches the probability of the more complicated scheme above. The problem is, however, that the outgoing directions leaving the medium, when escape is sampled, are not the distribution required for zero variance because we messed with the importance function outside of the volume. However, we can compute the exitant cosine distribution that the zero-variance walk does produce when starting from  $x$  and leaving in a single step,

$$p_e(x, \mu) = \frac{\int_0^\infty p_c(s) \Theta(-x - s\mu) ds}{\int_{-1}^0 \int_0^\infty p_c(s) \Theta(-x - s\mu) ds d\mu} = \frac{e^{\frac{x}{\mu} + x} (\mu - x)}{\mu}, \quad (56)$$

where  $\Theta(x)$  is the Heaviside Function. We can sample direction cosine  $\mu$  from Eq.(56) using

$$\mu = -\frac{x}{W_{productlog}\left(-\frac{e^{-x}x}{\xi - 1}\right)} \quad (57)$$

where  $W_{productlog}$  is the product log function, typically written as  $W$ . Combining these two results, the walk proceeds with the unclamped distance and angle decisions until escape is sampled. Then we back up to the last collision prior to escape, resample an outgoing direction using Eq.(56) and jump to the boundary along that path. The expected-value weight calculation for this escape sampling is a ratio of angle pdfs times a ratio of escape pdfs,

$$w_{esc} = \frac{1/2}{p_e(x, \mu)} \frac{X_c(-x/\mu)}{p_{esc\phi}(x)}. \quad (58)$$

We will see in the next section that this modified scheme is closely related to asymptotic guiding in a classical 3D half space and that resampled escape can greatly reduce the variance relative to the method originally presented for rendering [Křivánek and d'Eon 2014].

It is also fascinating to note that we have just derived two new zero variance estimators for classical scattering in the half rod, our first example above. Observe that if we enter the Gamma-2 half space by sampling a uniform (Lambertian) surface source, that the expected analog distance of the first collision is the simple exponential

$$2 \int_0^1 p_u(x/\mu) d\mu = e^{-x}. \quad (59)$$

From here, all displacements in the 3D space when projected onto the  $x$ -axis exactly behave as the classical exponential walk in 1D. And the final albedo of the 3D Gamma-2 half space under diffuse uniform illumination is exactly the same as the 1D classical rod:

$$2 \int_0^1 R(\mu) \mu = \frac{2}{\alpha} (1 - \sqrt{1 - \alpha}) - 1 \quad (60)$$

in agreement with (10). We also see the same probabilities for upwelling and downwelling directions in all three walks. This is a great example of how an importance sampling process can be achieved in many different ways with auxiliary dummy variables that place the simulation in a higher dimension space.

**Further Considerations:** We hope that our zero-variance estimators for the Gamma-2 GRT can add value in traditional rendering of classical media, despite the different free-path statistics. This hunch is based on limited testing of rendering objects with the diffuse BRDF for Gamma-2 GRT and comparing to Chandrasekhar's  $H$ -function BRDF for the classical medium. Both transport BRDFs exhibit a dusty appearance and significantly differ from the "CG" Lambertian appearance. We notice very similar appearance between the Gamma-2 and exponential BRDFs (Figure 10), suggesting that Gamma-2 may be a generally useful replacement for classical transport. There are several other reasons to consider this proposal. In addition to having an exact zero-variance estimator for thick flat geometry, the BRDF for Gamma-2 GRT also has an explicit expression, which we call the *diffusion transport* BRDF [d'Eon 2019b]

$$f_r(\theta_i, \theta_o) = \frac{\alpha}{4\pi} \left( \frac{H(\mu_i)H(\mu_o)}{\mu_i + \mu_o} \right)^2 \left( \frac{\mu_i^2 + 3\mu_i\mu_o + \mu_o^2}{\mu_i + \mu_o} - \frac{U_1}{2(1 + \mu_i)^2(1 + \mu_o)^2} \right) \quad (61)$$

where

$$\begin{aligned} U_1 = & (1 - \sqrt{1 - \alpha}) (\mu^2 + 3\mu_i\mu_o + 2\mu_o) (\mu_o^2 + 3\mu_i\mu_o + 2\mu_i) + \\ & \frac{\alpha\mu_i\mu_o}{\mu_i + \mu_o} (\mu_i^3 + \mu_o^3 + \mu_i\mu_o (2(\mu_i^2 + \mu_o^2 + 1) + 6\mu_i\mu_o + 3(\mu_i + \mu_o))) \end{aligned} \quad (62)$$

with the Picard  $H$  function given in Eq.(30), and  $\mu_i = \cos \theta_i, \mu_o = \cos \theta_o$ . This avoids the integrals required to evaluate the Milne  $H$  function in Chandrasekhar's BRDF. Also, this BRDF admits a simple closed-form albedo mapping. The diffuse albedo  $R$  of the Gamma-2 halfspace under uniform illumination is

$$R = \frac{\alpha}{(\sqrt{1 - \alpha} + 1)^2} \quad (63)$$

which easily inverts to single single-scattering albedo  $\alpha$  from diffuse albedo  $R$ ,

$$\alpha = \frac{4R}{(R + 1)^2}. \quad (64)$$

There may also be opportunity to apply some of the sampling distributions in this zero variance walk to different types of media with some appropriate fitting procedures.

## 6.6 Asymptotic (Dwivedi) Guiding

In the last two examples, we saw exact zero variance walks from absorbing half spaces with isotropic scattering. These were possible because the importance functions were known exactly and were simple expressions that admitted the required sampling manipulations. This is atypical of practical problems, even in plane geometry, so now we turn our attention to scenarios where we are forced to assume some approximate function for importance-to-escape; specifically, the approximation that results from taking the rigorous asymptotic diffusion term from the exact solution and discarding the transient portion. This method is highly effective for shielding calculations through optically thick shields because far from the boundaries, the transient terms in the exact importance function fall off and the resulting guiding becomes exact. In our previous work we attributed this method to Dwivedi [1982] but it appears that the original proposal of asymptotic guiding was earlier [Lanore 1971; Marchuk et al. 2013]. See also several more recent works on the topic [Meng et al. 2016; Medvedev and Mikhailov 2008].



(a) Lambertian

(b) Chandrasekhar

(c) Diffusion Transport

**Figure 10:** Comparison of 3 diffuse BRDFs. Chandrasekhar’s BRDF and the new diffusion transport BRDF for Gamma-2 GRT look very similar, but the latter has a zero-variance random walk and simple albedo mapping.

**Motivation** Like the examples above, the asymptotic guiding zero-variance method begins by first trying to find an exact importance-to-escape function  $W(x)$ . For classical exponential transport in a 3D half space with isotropic scattering the Milne kernel arises and is singular. Here, the exact importance function for escape is not a simple exponential. Instead, we find Case’s exact solution involving a discrete asymptotic diffusion term (an exponential with a complicated constant) and a transient term that is an integral of exponentials [Case 1960; McCormick and Kuščer 1973; d’Eon 2016; d’Eon and McCormick 2019]. This relates to a rich set of results that began with observations by Davison [2000] and later expanded upon by Case [1960]. The importance function that results can also be equivalently found via the Wiener Hopf method. The final solution is expressed as a Fourier inversion, and via contour manipulation the discrete portion of the answer pops out as the residue of a pole, creating a diffusion result—but not the  $P_1$  or “classical” diffusion result—the diffusion length is different. For anisotropic scattering the same things happens but more than one discrete diffusion term appear as the phase function gets increasingly peaked.

We now have the exact answer at hand, but an issue arises. The transient portion of the importance function involves integrals of eigenfunctions that are singular in direction<sup>4</sup> and sometimes negative and so are not amenable to guiding. This has motivated the approximation of discarding the transient term and assuming the discrete term well approximates the full solution. For escaping a 3D half space, this becomes simply the translationally invariant  $W(x) = e^{-x/\nu_0}$ , where  $\nu_0$  is the discrete eigenvalue of the Milne kernel.

**Discrete Eigenvalue** Having made the approximation for  $W(x)$  we proceed with the derivation analogous to the previous example for Gamma-2 GRT. The diffusion length we want follows from normalization of the guided angle sampling distribution

$$\phi(\mu, \nu_0) = \frac{\alpha}{2} \int_0^\infty p_c(s) e^{-s\mu\nu_0/\nu_0} = \frac{c}{2} \left( \frac{1}{1 + \mu/\nu_0} \right). \quad (65)$$

Normalizing this polar angle distribution produces the dispersion equation

$$1 = \frac{\alpha\nu_0 \tanh^{-1} \left( \frac{\ell}{\nu_0} \right)}{\ell}. \quad (66)$$

---

<sup>4</sup>The eigen expansion of the angular collision rate and radiance inside the volume must include singularities and generalized distribution “functions” because of the reduced-intensity term from the source at the boundary, which is a delta in direction. In fact, even with a diffuse source at the boundary, the exact radiance in the volume at each depth is expressed as a superposition of the singular distributions even though the final result is smooth.

Our approximate importance  $W(x)$  follows from finding the positive real root  $\nu_0$  of this equation. Eq.(66) is often called a transcendental equation but actually has a closed-form solution [Siewert 1980; d'Eon and McCormick 2019]. The exact solution is not numerically convenient, so we recommend the following approximation, with a relative error bounded by 0.0001

$$\nu_0 \approx \ell \frac{1}{\sqrt{1 - \alpha^{2.44294 - 0.0215813\alpha + \frac{0.578637}{\alpha}}}}. \quad (67)$$

Equation (67) is an order of magnitude more accurate than other piecewise approximations [Winslow 1968; Harel et al. 2020].

The remaining details of the asymptotic guiding scheme are found in several works [Dwivedi 1982; Křivánek and d'Eon 2014; Meng et al. 2016; Lanore 1971; Marchuk et al. 2013]. We will touch upon various select topics related to the method and refer the reader to these works for full details.

**Weight Factor Simplification** It is worth mentioning why this particular form of approximate importance function works so well and why, despite the approximation, undesired weight fluctuations that plagued earlier attempts to apply the exponential transform don't arise for this scheme. This happens because of a synergistic cancellation between weight factors in the direction and step length sampling steps [Dwivedi and Gupta 1986]. Referring now briefly to the notation in [Křivánek and d'Eon 2014], the weight adjustment when sampling stretched transition distance picks up a multiplicative weight correction of

$$w_s = \frac{e^{-s}}{\sigma'_t e^{-s\sigma'_t}}. \quad (68)$$

The angle selection incurs a multiplicative weight correction of

$$w_\mu = \frac{1}{2} \frac{1}{\frac{\alpha}{2} \frac{1}{1-\mu/\nu_0}}. \quad (69)$$

The eigenfunction  $\phi(\mu, \nu_0)$  that appears in the denominator of  $w_\mu$  mostly cancels with the  $\sigma'_t$  in  $w_s$ . When using fitted or tabulated distributions for angle and step lengths that do not exhibit this precise cancellation there can be low number of paths where significantly high particle weights arise.

We can further simplify the final weight  $w_o$  after angle selection, absorption and transition, expressed as a multiplication of the previous weight  $w_i$  before collision with the other weight adjustments, including the single-scattering albedo multiplier  $\alpha$ , sees significant cancellation, giving simply

$$w_o = w_i * \alpha * w_s * w_\mu = w_i * \frac{\xi_s^{-1 + \frac{\nu_0}{\sigma_t(\nu_0 - \mu)}}}{\sigma_t} \quad (70)$$

where  $\xi_s$  was the random number used to sample displacement  $s$ .

**Curved Geometry and General Lighting** For general shapes, multiple importance sampling (MIS) can be used to combine analog/unguided sampling decisions with guided ones [Křivánek and d'Eon 2014]. This avoids the increased variance in regions with high curvature where particles exit the medium where the importance function was expected to be low. Figure 11 illustrates the impact of this combination of classical and guided estimators. Figure 12 shows the performance of the method under general lighting. Despite not sampling the product of BSSRDF and lighting, the reduction of the absorption variance is significant. Also, the average path length is reduced in guiding paths out of the medium more often than the classical walk. The histograms over path-length for both methods are compared in Figure 14 and examples scattering histories are shown in Figure 13 to more clearly illustrate how increased absorption alters the set of sampled paths. For expanded results on handling general light and geometry see [Meng et al. 2016].



**Figure 11:** MIS between guided and classical sampling.

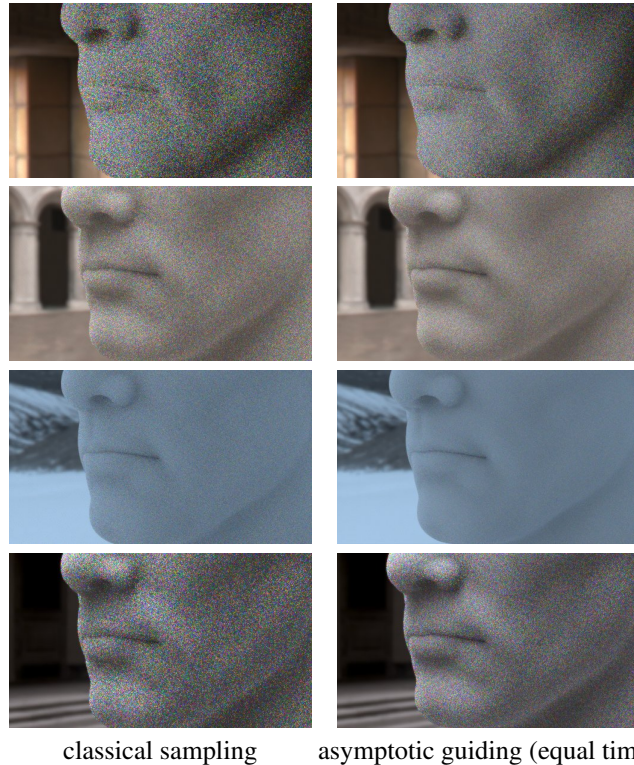


**Figure 12:** A gray material with isotropic scattering and single-scattering albedo of 0.943 under a variety of illumination conditions. The images rendered with classical sampling use 100 samples/pixel while with guided sampling can perform 50% more samples/pixel in the same time. The guided sampling assumes uniform hemispherical illumination everywhere on the surface and flat geometry yet still improves the convergence rate of random walk SSS for curved geometry under arbitrary illumination conditions.

### 6.6.1 Fresnel Boundaries

Largely missing from the zero-variance literature is the role of general BSDFs at medium boundaries and the impact of this on the zero-variance scheme. To see the influence of BSDF interactions on the derivation, consider the half space: in the downwelling directions the procedure is as before. We can think of upward angle selection as before but now the probability to leave a collision in an upwelling direction depends upon the more complicated result of importance from future collisions up to the boundary plus a new term that considers reflections back into the medium and the total escape probability, which is now a general BSDF integral over the exitant hemisphere,

$$\int_{4\pi} f_s(\omega_i, \omega) |\omega \cdot \vec{n}| W_b(\omega) d\omega \quad (71)$$

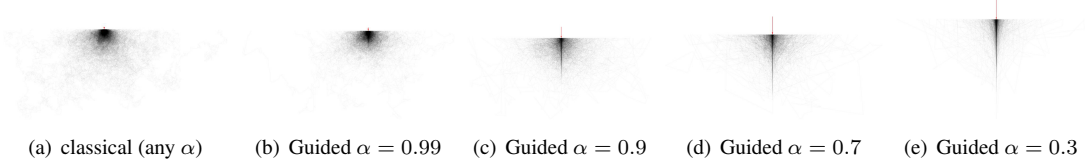


**Figure 13:** In each subfigure we show 2000 randomly sampled paths created using either classical volumetric sampling (a) or the Dwivedi sampling scheme (b-e). The figures have differing scales—the red arrow is one mean-free-path long and indicates the illumination position and direction. All paths continue inside the semi-infinite medium with isotropic scattering until an escape is sampled. Each path is rasterized with the same opacity, regardless of sample weight. Irrespective of absorption level (the value of  $\alpha$ ), the classical scheme samples the wide distribution of paths shown in (a), even though many of these paths are heavily absorbed and contribute negligible energy to the final result. Russian roulette helps avoid this wasteful sampling, but increases variance of each sample as a consequence. The Dwivedi sampling scheme we use adapts to the absorption levels of the medium and creates shorter, important paths more often, while simultaneously decreasing the variance of each sample.

where we define  $W_b(\omega)$  as the importance function that is the probability that a particle leaving the boundary along direction  $\omega$  eventually escapes, which is

$$W_b(\omega) = \begin{cases} \int_0^\infty p_u(s)W(s\mu)ds, & \omega \text{ is downwelling} \\ 1, & \omega \text{ is upwelling.} \end{cases} \quad (72)$$

We also have a new sampling decision to make upon jumping to the boundary during the walk, which is guided sampling of the BSDF. As in the derivation of the other steps, we start with the analog sampling distribution, the BSDF itself, and multiply it by the corresponding importance function  $W_b(\omega)$  and normalize the result. Thus, having arrived at the boundary from inside *from* direction  $\omega_i$  we must sample guided direction  $\omega$  leaving the boundary from the normalization of

$$\int_{4\pi} f_s(\omega_i, \omega) W_b(\omega) |\cos \theta_o| d\omega. \quad (73)$$

For anything but a smooth Fresnel interface, this becomes a complicated problem to sample analytically. Novel methods will be required to efficiently perform this sampling for rough dielectric interfaces with multiple scattering [Dupuy et al. 2016; Heitz et al. 2016].

### 6.6.2 Asymptotic Guiding with Exit Resampling

We briefly tested the exit resampling approach from the Gamma-2 GRT estimator in the case of classical exponential transport in a 3D half space with isotropic scattering and indexed-matched smooth boundary. The approach uses the procedure described in prior work [Křivánek and d’Eon 2014; Meng et al. 2016] but when the translationally-invariant sampling produces escape, we backup and resample outgoing polar angle, now from

$$\frac{e^{\frac{x}{\mu}+x}}{1 - e^x x E_1(x)} \quad (74)$$

where  $E_1(x)$  is the exponential integral function. We sampled this using naive rejection and performed some tests viewing flat patches of half space under uniform white illumination (Figure 15). We found the reduction in variance for resampled Dwivedi vs Dwivedi ranging from 10 times lower for  $\alpha = 0.95$  to 45 times lower for  $\alpha = 0.3$ . We expect the additional sampling time is mostly due to the naive rejection sampling.

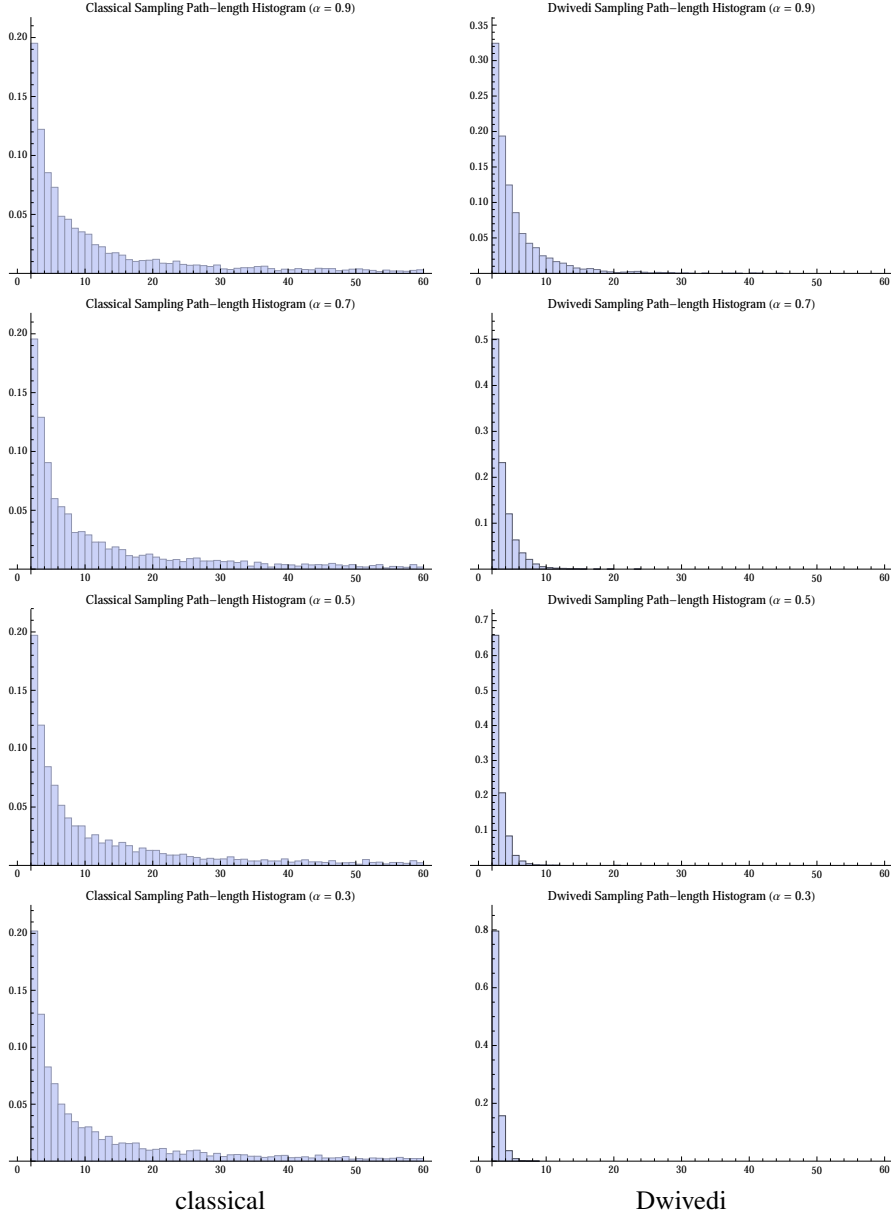


**Figure 14:** Comparison of the distributions of path lengths (in terms of path segment count) generated by classical sampling (without Russian roulette) and our application of Dwivedi sampling for the problem of reflection of normally-incident illumination from an isotropically-scattering semi-infinite medium. The zero-variance-based Dwivedi sampling scheme generates much shorter paths on average whilst simultaneously decreasing variance (as opposed to Russian roulette). The method automatically adapts to the single-scattering albedo  $\alpha$  of the medium.

This suggests that much of the remaining variance in asymptotic guiding is not so much from errors in the importance function inside the medium but from not clamping it to 1 outside. While the exit resampling procedure would not be easy to apply in general curved geometry, this result suggests that finding a clamped exponential sampling scheme would be well worth the effort.

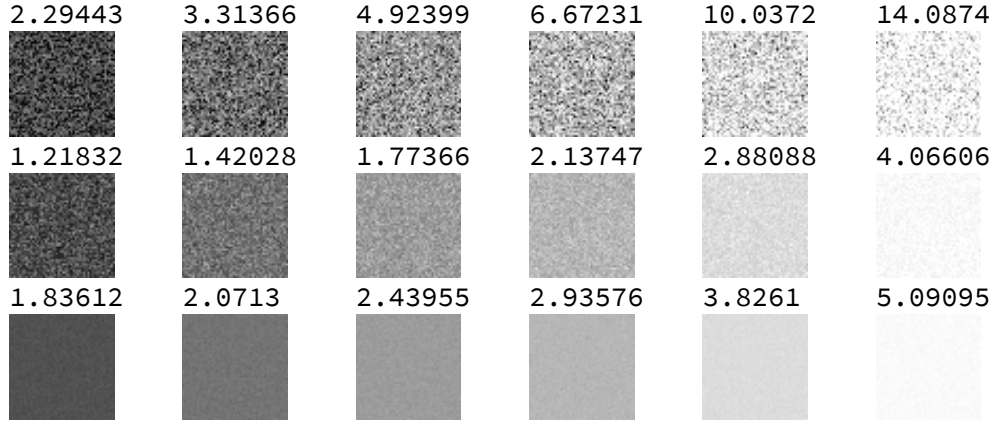


**Figure 15:** Normally-viewed patches of a 3D half space under uniform white illumination rendered with three estimators, classical (top), standard Dwivedi (middle), and Dwivedi with exit resampling (bottom). Single scattering albedo from left to right: 0.3, 0.5, 0.7, 0.8, 0.9, 0.95. Each patch is 50 by 50 pixels with 5 samples per pixel. Timings in seconds above each patch. Gamma correction of 2.0.

### 6.6.3 Asymptotic Guiding in GRT

In Section 6.5.2 we considered a form of GRT in 3D with Gamma random flights that admits an exactly zero-variance walk analytically. We also saw that asymptotic guiding was not a zero-variance walk, but could be corrected with exit resampling. We chose this form of GRT because of its mathematical properties. It is the unique form of GRT in 3D with isotropic scattering where the collision density inside the volume exactly satisfies a diffusion equation [d’Eon 2013]. Diffusion is *not an approximation* in Gamma-2 3D!. While helpful for illustrating how guided walks are derived, we are unaware of any specific microstructure that would motivate these exact free-flight statistics. It likely corresponds to a short-length negative correlation of some kind. For more general forms of GRT motivated by observed spatial variability in the volume coefficients, diffusion will not be an exact answer and asymptotic guiding or alternative approximate importance functions will be needed.

One popular [Davis 2006; Wrenninge et al. 2017; Jarabo et al. 2018; Bitterli et al. 2018] and practical GRT model for random media that includes long-range correlations and power-law asymptotics, while avoiding the more complex Mittag-Leffler functions that satisfy fractional diffusion equations [Liemert and Kienle 2018], derives from a continuum model of random scattering-particle number densities drawn from a Gamma distribution, producing [d’Eon 2018; Jarabo et al. 2018]

$$p_c(s) = a(a+1)\ell(a\ell)^a(a\ell + s)^{-a-2}, \quad a > 0 \quad (75)$$

where the mean free path between collisions is  $\ell$  and a shape parameter  $a > 0$  adjusts the correlation between scattering events with classical exponential media recovered in the limit  $a \rightarrow \infty$ . The intercollisions distribution  $p_c(s)$  does not decay exponentially due to the long-range nature of the correlations. For isotropic scattering in 3D plane geometry, this leads to a discrete Case eigenfunction derivation of [d’Eon 2019a]

$$\phi(\mu, \nu_0) = \frac{\alpha}{2} \int_0^\infty p_c(s) e^{-s\mu/\nu_0} = \frac{\alpha}{2}(a+1)e^{\frac{a\mu\ell}{\nu_0}} E_{a+2}\left(\frac{a\ell\mu}{\nu_0}\right), \quad 0 < \mu \leq 1. \quad (76)$$

The integral diverges, however, in the upwelling directions, so the exponential, and unbounded, importance function could only be used to guide downwelling direction sampling. This illustrates a failure

of the approach of Case that assumes exponentially-decaying kernels. For this class of flights, the dispersion equation admits a pair of complex roots, but no real  $\nu_0$  eigenvalue exists. It is an interesting open problem to investigate what asymptotic importance function might apply in this setting and if the Mittag-Leffler functions that generalize the exponential distribution make an appearance here.

#### 6.6.4 Anisotropic Scattering

Including anisotropic scattering in guiding-to-escape walk derivations complicates things substantially. The importance function for escape upon entering a collision depends on the cosine  $\mu$  as well as the position. The direction sampling is much more complicated, requiring importance to leave a collision  $W_o(x, \omega)$  in terms of general direction and to sample the product of this distribution with the phase function, for which the normalization factor is typically impossible to determine analytically. To address this issue Lanore [1971] offers some insight. We recommend Ueki and Larsen [1998] for more details on linearly and quadratically-anisotropic phase functions and procedures for sampling the product of the phase function and the importance function, and also [Marchuk et al. 2013].

### 6.7 General Tips

**Validating the Walk** When deriving analytic importance functions or fitting tabulated data from adjoint Monte Carlo simulation it can be helpful to ensure the correctness of these solutions using forward Monte Carlo simulation to simulate exactly the probability that is needed at a given sampling step. For example, if we require  $W(x, \omega)$ , the probability for a single particle to escape the medium upon entering a collision at  $x$  into direction  $\omega$ , then we would start a Monte Carlo random walk at  $x$  that begins by sampling a collision right away, applying  $\alpha$  and sampling the phase function with direction  $\omega$  before stepping through the volume. Testing this for a variety of absorption levels  $\alpha_s$ , depths  $x$  and directions  $\omega$  will validate any adjoint fittings or derivations. If  $W$  is off by even a small forgotten factor of  $\alpha$ , the resultant walk will continue to show considerable variance.

Another debugging tool that we found helpful is to check at each collision entry that  $wW(x, \omega) = R$ . When an implementation that should be zero variance is not, this can help identify what step is causing the issue. This can also help identify what steps in an almost-zero-variance walk are causing the most variance.

Finally, the walk should always reduce to the classical method of analog sampling plus implicit capture when absorption is removed,  $\alpha = 1$ .

**Russian Roulette** Russian roulette is a common device for reducing the lengths of long random walks when the weight becomes low [Arvo and Kirk 1990]. However, if the importance function and its use to guide the random walk are both accurate, then it is most likely that Roulette will only increase variance and possibly reduce efficiency. Hero wavelength sampling and MIS complicate this conclusion, however. We recommend undertaking a thorough analysis for your particular problem to determine how and when to employ roulette with guided walks.

### 6.8 Acknowledgements

I am grateful to Jaroslav for travelling to New Zealand to work together with me on this topic in what would become one of the most rewarding and thrilling collaborations I've been lucky to enjoy. He approached the neutron transport literature with great excitement and fascination and with an unwavering determination to find an exactly zero-variance walk. When our sandbox experiments showed the potential of Dwivedi's asymptotic guiding for half space problems he saw exactly how to defeat the deficiencies of the method in curved geometry with MIS and had it working in Manuka within a week—a feat that would certainly have not happened without him. We lost a gifted researcher from whom we learned so much, and also a dear friend.

## References

- ANISIMOV, O., AND FUKSHANSKY, L. 1992. Stochastic radiation in macroheterogeneous random optical media. *Journal of Quantitative Spectroscopy and Radiative Transfer* 48, 2, 169–186. [https://doi.org/10.1016/0022-4073\(92\)90087-K](https://doi.org/10.1016/0022-4073(92)90087-K).
- ARVO, J., AND KIRK, D. 1990. Particle transport and image synthesis. *ACM SIGGRAPH Computer Graphics* 24, 4, 63–66. <https://doi.org/10.1145/97879.97886>.
- AUDIC, S., AND FRISCH, H. 1993. Monte-Carlo simulation of a radiative transfer problem in a random medium: Application to a binary mixture. *Journal of Quantitative Spectroscopy and Radiative Transfer* 50, 2, 127–147. [https://doi.org/10.1016/0022-4073\(93\)90113-V](https://doi.org/10.1016/0022-4073(93)90113-V).
- BHAN, K., AND SPANIER, J. 2007. Condensed history monte carlo methods for photon transport problems. *Journal of computational physics* 225, 2, 1673–1694. <https://doi.org/10.1016/j.jcp.2007.02.012>.
- BITTERLI, B., RAVICHANDRAN, S., MÜLLER, T., WRENNINGE, M., NOVÁK, J., MARSCHNER, S., AND JAROSZ, W. 2018. A radiative transfer framework for non-exponential media. *ACM Transactions on Graphics* 37, 6. <https://doi.org/10.1145/3272127.3275103>.
- BORSHUKOV, G., AND LEWIS, J. P. 2003. Realistic human face rendering for “The Matrix Reloaded”. In *ACM SIGGRAPH Sketches and Applications*, ACM, 1. <https://doi.org/10.1145/1198555.1198593>.
- BURRUS, W. 1958. How channeling between chunks raises neutron transmission through boral. *Nucleonics (US) Ceased publication* 16.
- BURRUS, W. 1960. Radiation transmission through boral and similar heterogeneous materials consisting of randomly distributed absorbing chunks. Tech. rep., Oak Ridge National Lab., Tenn. <https://doi.org/10.2172/4196641>.
- CASE, K. 1960. Elementary solutions of the transport equation and their applications\*. *Annals of Physics* 9, 1, 1–23. [https://doi.org/10.1016/0003-4916\(60\)90060-9](https://doi.org/10.1016/0003-4916(60)90060-9).
- CHANDRASEKHAR, S. 1960. *Radiative Transfer*. Dover.
- CHIANG, M. J.-Y., KUTZ, P., AND BURLEY, B. 2016. Practical and controllable subsurface scattering for production path tracing. In *ACM SIGGRAPH 2016 Talks*. 1–2. <https://doi.org/10.1145/2897839.2927433>.
- CHRISTENSEN, P., FONG, J., SHADE, J., WOOTEN, W., SCHUBERT, B., KENSLER, A., FRIEDMAN, S., KILPATRICK, C., RAMSHAW, C., BANNISTER, M., RAYNER, B., BROUILLAT, J., AND LIANI, M. 2018. Renderman: An advanced path-tracing architecture for movie rendering. *ACM Trans. Graph.* 37, 3 (Aug.). <https://doi.org/10.1145/3182162>.
- CHRISTENSEN, P. H. 2003. Adjoints and importance in rendering: An overview. *IEEE Transactions on Visualization and Computer Graphics* 9, 3, 329–340. <https://doi.org/10.1109/TVCG.2003.1207441>.
- CHRISTENSEN, P. H. 2015. An approximate reflectance profile for efficient subsurface scattering. In *ACM SIGGRAPH 2015 Talks*. 1–1. <https://doi.org/10.1145/2775280.2792555>.
- COVEYOU, R., CAIN, V., AND YOST, K. 1967. Adjoint and Importance in Monte Carlo Application. *Nucl. Sci. Eng.* 27, 1, 219–234. <https://doi.org/10.13182/NSE67-A18262>.

- DAVIS, A. B., AND MINEEV-WEINSTEIN, M. B. 2011. Radiation propagation in random media: From positive to negative correlations in high-frequency fluctuations. *Journal of Quantitative Spectroscopy and Radiative Transfer* 112, 4, 632–645. <https://doi.org/10.1016/j.jqsrt.2010.10.001>.
- DAVIS, A. B., AND XU, F. 2014. A generalized linear transport model for spatially correlated stochastic media. *Journal of Computational and Theoretical Transport* 43, 1-7, 474–514. <https://doi.org/10.1080/23324309.2014.978083>.
- DAVIS, A. B. 2006. Effective propagation kernels in structured media with broad spatial correlations, illustration with large-scale transport of solar photons through cloudy atmospheres. In *Computational Methods in Transport*. Springer, 85–140. [https://doi.org/10.1007/3-540-28125-8\\_5](https://doi.org/10.1007/3-540-28125-8_5).
- DAVISON, B. 2000. Angular distribution due to an isotropic point source and spherically symmetrical eigensolutions of the transport equation (MT-112). *Progress in Nuclear Energy* 36, 3, 323 – 365. Nuclear Reactor Theory in Canada 1943-1946. [https://doi.org/10.1016/S0149-1970\(00\)00012-3](https://doi.org/10.1016/S0149-1970(00)00012-3).
- DENG, H., WANG, B., WANG, R., AND HOLZSCHUCH, N. 2020. A practical path guiding method for participating media. *Computational Visual Media*, 1–15. <https://doi.org/10.1007/s41095-020-0160-1>.
- D'EON, E., AND IRVING, G. 2011. A quantized-diffusion model for rendering translucent materials. In *ACM Transactions on Graphics (TOG)*, vol. 30, ACM, 56. <https://doi.org/10.1145/2010324.1964951>.
- D'EON, E., AND MCCORMICK, N. J. 2019. Radiative transfer in half spaces of arbitrary dimension. *Journal of Computational and Theoretical Transport* 48, 7, 280–337. <https://doi.org/10.1080/23324309.2019.1696365>.
- D'EON, E., LUEBKE, D., AND ENDERTON, E. 2007. Efficient rendering of human skin. In *Rendering Techniques*, 147–157. <https://doi.org/10.5555/2383847.2383869>.
- D'EON, E. 2013. Rigorous Asymptotic and Moment-Preserving Diffusion Approximations for Generalized Linear Boltzmann Transport in Arbitrary Dimension. *Transport Theory and Statistical Physics* 42, 6-7, 237–297. <https://doi.org/10.1080/00411450.2014.910231>.
- D'EON, E. 2014. A Dual-beam 3D Searchlight BSSRDF. *ACM SIGGRAPH 2014 Talks* 65, 1, 1. <http://doi.acm.org/10.1145/2614106.2614140>.
- D'EON, E. 2016. A Hitchhiker's Guide to Multiple Scattering. (*self published*). <http://eugenedeon.com/hitchhikers>.
- D'EON, E. 2018. A reciprocal formulation of nonexponential radiative transfer. 1: Sketch and motivation. *Journal of Computational and Theoretical Transport*. <https://doi.org/10.1080/23324309.2018.1481433>.
- D'EON, E. 2019. A reciprocal formulation of nonexponential radiative transfer. 2: Monte-Carlo Estimation and Diffusion Approximation. *Journal of Computational and Theoretical Transport* 48, 6, 201–262. <https://doi.org/10.1080/23324309.2019.1677717>.
- D'EON, E. 2019. The Albedo Problem in Nonexponential Radiative Transfer. In *International Conference on Transport Theory (ICTT-26) - Abstracts*. <https://www.researchgate.net/publication/333325137>.
- DONNER, C., AND JENSEN, H. W. 2005. Light Diffusion in Multi-Layered Translucent Materials. *ACM Trans. Graphic.* 24, 3, 1032–1039. <https://doi.org/10.1145/1186822.1073308>.

- DONNER, C., WEYRICH, T., D'EON, E., RAMAMOORTHI, R., AND RUSINKIEWICZ, S. 2008. A layered, heterogeneous reflectance model for acquiring and rendering human skin. In *SIGGRAPH Asia '08: ACM SIGGRAPH Asia 2008 papers*, ACM, New York, NY, USA, 1–12. <https://doi.org/10.1145/1457515.1409093>.
- DUPUY, J., HEITZ, E., AND D'EON, E. 2016. Additional progress towards the unification of microfacet and microflake theories. In *EGSR (EI&I)*, 55–63. <https://doi.org/10.5555/3056507.3056519>.
- DUTKA, J. 1985. On the problem of random flights. *Archive for history of exact sciences* 32, 3, 351–375. <https://doi.org/10.1007/BF00348451>.
- DWIVEDI, S., AND GUPTA, H. 1986. Biasing parameter limits for synergistic monte carlo in deep-penetration calculations. *Nuclear Science and Engineering* 92, 4, 545–549. <https://doi.org/10.13182/NSE86-A18611>.
- DWIVEDI, S. 1982. A new importance biasing scheme for deep-penetration Monte Carlo. *Annals of Nuclear Energy* 9, 7, 359–368. [https://doi.org/10.1016/0306-4549\(82\)90038-X](https://doi.org/10.1016/0306-4549(82)90038-X).
- FASCIONE, L., HANIKA, J., LEONE, M., DROSKE, M., SCHWARZHaupt, J., DAVIDovič, T., WEIDLICH, A., AND MENG, J. 2018. Manuka: A batch-shading architecture for spectral path tracing in movie production. *ACM Transactions on Graphics (TOG)* 37, 3, 1–18. <https://doi.org/10.1145/3182161>.
- FELLER, W. 1971. *An Introduction to Probability theory and its application Vol II*. John Wiley and Sons.
- FLECK, J., AND CANFIELD, E. 1984. A random walk procedure for improving the computational efficiency of the implicit monte carlo method for nonlinear radiation transport. *Journal of Computational Physics* 54, 3, 508–523. [https://doi.org/10.1016/0021-9991\(84\)90130-X](https://doi.org/10.1016/0021-9991(84)90130-X).
- FREDERICKX, R., AND DUTRÉ, P. 2017. A forward scattering dipole model from a functional integral approximation. *ACM Transactions on Graphics (TOG)* 36, 4, 109. <https://doi.org/10.1145/3072959.3073681>.
- FRISCH, U. 1968. Wave propagation in random media. In *Probabilistic methods in applied mathematics*, A. Bharucha-Reid, Ed. Academic Press, 75–198.
- FRISVAD, J. R., CHRISTENSEN, N. J., AND JENSEN, H. W. 2007. Computing the Scattering Properties of Participating Media Using Lorenz-Mie Theory. In *ACM SIGGRAPH 2007 Papers*, Association for Computing Machinery, New York, NY, USA, SIGGRAPH '07, 60–es. <https://doi.org/10.1145/1275808.1276452>.
- FRISVAD, J. R., HACHISUKA, T., AND KJELDSEN, T. K. 2014. Directional dipole model for subsurface scattering. *ACM Transactions on Graphics (TOG)* 34, 1, 1–12. <https://doi.org/10.1145/2682629>.
- FUKSHANSKY, L. 1987. Absorption statistics in turbid media. *Journal of quantitative spectroscopy and radiative transfer* 38, 5, 389–406. [https://doi.org/10.1016/0022-4073\(87\)90033-1](https://doi.org/10.1016/0022-4073(87)90033-1).
- GEORGIEV, I., IZE, T., FARNSWORTH, M., MONTOYA-VOZMEDIANO, R., KING, A., LOMMEL, B. V., JIMENEZ, A., ANSON, O., OGAKI, S., JOHNSTON, E., HERUBEL, A., RUSSELL, D., SERVANT, F., AND FAJARDO, M. 2018. Arnold: A brute-force production path tracer. *ACM Trans. Graph.* 37, 3 (Aug.). <https://doi.org/10.1145/3182160>.
- GROSJEAN, C. 1951. The Exact Mathematical Theory of Multiple Scattering of Particles in an Infinite Medium. *Memoirs Kon. Vl. Ac. Wetensch.* 13, 36.

- GUO, Y., HAŠAN, M., AND ZHAO, S. 2018. Position-free monte carlo simulation for arbitrary layered bsdfs. *ACM Transactions on Graphics (TOG)* 37, 6, 1–14. <https://doi.org/10.1145/3272127.3275053>.
- HABEL, R., CHRISTENSEN, P. H., AND JAROSZ, W. 2013. Photon beam diffusion: a hybrid Monte Carlo method for subsurface scattering. In *Computer Graphics Forum*, vol. 32, Wiley Online Library, 27–37. <https://doi.org/10.1111/cgf.12148>.
- HAGHIGHAT, A., AND WAGNER, J. C. 2003. Monte Carlo variance reduction with deterministic importance functions. *Progress in Nuclear Energy* 42, 1, 25–53. [https://doi.org/10.1016/S0149-1970\(02\)00002-1](https://doi.org/10.1016/S0149-1970(02)00002-1).
- HANRAHAN, P., AND KRUEGER, W. 1993. Reflection from layered surfaces due to subsurface scattering. In *Proceedings of ACM SIGGRAPH 1993*, 164–174. <https://doi.org/10.1145/166117.166139>.
- HAREL, R., BUROV, S., AND HEIZLER, S. I. 2020. The Time-Dependent Asymptotic  $P_N$  Approximation for the Transport Equation. *arXiv preprint arXiv:2006.11784*. <https://arxiv.org/abs/2006.11784v1>.
- HEITZ, E., HANIKA, J., D'EON, E., AND DACHSBACHER, C. 2016. Multiple-scattering microfacet BSDFs with the Smith model. *ACM Transactions on Graphics (TOG)* 35, 4, 58. <https://doi.org/10.1145/2897824.2925943>.
- HOFFMAN, W. 1964. Wave propagation in a general random continuous medium. *Proc. Symp. Appl. Math.* 16, 117–144.
- HOOGENBOOM, J. 1981. A practical adjoint Monte Carlo technique for fixed-source and eigenfunction neutron transport problems. *Nuclear Science and Engineering* 79, 4, 357–373. <https://doi.org/10.13182/NSE81-A21387>.
- HOOGENBOOM, E. 2008. Zero-Variance Monte Carlo Schemes Revisited. *Nucl. Sci. Eng.* 160, 1, 1–22. <https://doi.org/10.13182/NSE160-01>.
- HOOGENBOOM, J. 2008. The Two-Direction Neutral-Particle Transport Model: A Useful Tool for Research and Education. *Transport Theory and Statistical Physics* 37, 1, 65–108. <https://doi.org/10.1080/00411450802271791>.
- ISHIMARU, A. 1978. *Wave Propagation and Scattering in Random Media*. Oxford University Press.
- IVANOV, V. 1994. Resolvent method: exact solutions of half-space transport problems by elementary means. *Astronomy and Astrophysics* 286, 328–337. <https://ui.adsabs.harvard.edu/abs/1994A&A...286..328I>.
- JARABO, A., ALIAGA, C., AND GUTIERREZ, D. 2018. A radiative transfer framework for spatially-correlated materials. *ACM Transactions on Graphics* 37, 4, 14. <https://doi.org/10.1145/3197517.3201282>.
- JENSEN, H. W., MARSCHNER, S. R., LEVOY, M., AND HANRAHAN, P. 2001. A practical model for subsurface light transport. In *Proceedings of ACM SIGGRAPH 2001*, 511–518. <https://doi.org/10.1145/383259.383319>.
- KAHN, H. 1956. Applications of monte carlo. Tech. Rep. RM-1237-AEC. [https://www.rand.org/pubs/research\\_memoranda/RM1237.html](https://www.rand.org/pubs/research_memoranda/RM1237.html).
- KIRK, J. 1975. A theoretical analysis of the contribution of algal cells to the attenuation of light within natural waters I. General treatment of suspensions of pigmented cells. *New phytologist* 75, 1, 11–20. <https://doi.org/10.1111/j.1469-8137.1975.tb01366.x>.

- KULLA, C., CONTY, A., STEIN, C., AND GRITZ, L. 2018. Sony Pictures Imageworks Arnold. *ACM Trans. Graph.* 37, 3 (Aug.). <https://doi.org/10.1145/3180495>.
- KŘIVÁNEK, J., AND D'EON, E. 2014. A Zero-variance-based sampling scheme for Monte Carlo subsurface scattering. *ACM SIGGRAPH 2014 Talks* 66, 1, 1. <https://doi.org/10.1145/2614106.2614138>.
- LAFORTUNE, E. P., AND WILLEMS, Y. D. 1996. Rendering participating media with bidirectional path tracing. In *Rendering Techniques*, 91–100. [https://doi.org/10.1007/978-3-7091-7484-5\\_10](https://doi.org/10.1007/978-3-7091-7484-5_10).
- LANORE, J.-M. 1971. Weighting and Biasing of a Monte Carlo Calculation for Very Deep Penetration of Radiation. *Nucl. Sci. Eng.* 45, 1, 66–72. <https://doi.org/10.13182/NSE71-A20346>.
- LARMIER, C., HUGOT, F.-X., MALVAGI, F., MAZZOLO, A., AND ZOIA, A. 2017. Benchmark solutions for transport in  $d$ -dimensional Markov binary mixtures. *Journal of Quantitative Spectroscopy and Radiative Transfer* 189, 133–148. <https://doi.org/10.1016/j.jqsrt.2016.11.015>.
- LARSEN, E. W., AND VASQUES, R. 2011. A generalized linear Boltzmann equation for non-classical particle transport. *Journal of Quantitative Spectroscopy and Radiative Transfer* 112, 4, 619–631. <https://doi.org/10.1016/j.jqsrt.2010.07.003>.
- LIEMERT, A., AND KIENLE, A. 2013. Exact and efficient solution of the radiative transport equation for the semi-infinite medium. *Scientific Reports* 3. <https://doi.org/10.1038/srep02018>.
- LIEMERT, A., AND KIENLE, A. 2018. Fractional radiative transport in the diffusion approximation. *Journal of Mathematical Chemistry* 56, 2, 317–335. <https://doi.org/10.1007/s10910-017-0792-2>.
- LU, B., AND TORQUATO, S. 1992. Lineal-path function for random heterogeneous materials. *Physical Review A* 45, 2, 922. <https://doi.org/10.1103/PhysRevA.45.922>.
- MACHIDA, M., PANASYUK, G., SCHOTLAND, J., AND MARKEL, V. 2010. The green's function for the radiative transport equation in the slab geometry. *Journal of Physics A: Mathematical and Theoretical* 43, 065402. <https://doi.org/10.1088/1751-8113/43/6/065402>.
- MARCHUK, G. I., MIKHAILOV, G. A., NAZARELIEV, M., DARBINJAN, R. A., KARGIN, B. A., AND ELEPOV, B. S. 2013. *The Monte Carlo methods in atmospheric optics*, vol. 12. Springer.
- MCCORMICK, N., AND KUŠČER, I. 1973. Singular eigenfunction expansions in neutron transport theory. In *Advances in Nuclear Science and Technology*, Academic Press, E. J. Henley and J. Lewins, Eds., vol. 7, 181–282. <https://doi.org/10.1016/B978-0-12-029307-0.50010-X>.
- MEDVEDEV, I., AND MIKHAILOV, G. 2008. A new criterion for finiteness of weight estimator variance in statistical simulation. In *Monte Carlo and Quasi-Monte Carlo Methods 2006*. Springer, 561–576. [https://doi.org/10.1007/978-3-540-74496-2\\_33](https://doi.org/10.1007/978-3-540-74496-2_33).
- MENG, J., HANIKA, J., AND DACHSBACHER, C. 2016. Improving the Dwivedi sampling scheme. In *Computer Graphics Forum*, vol. 35, Wiley Online Library, 37–44. <https://doi.org/10.1111/cgf.12947>.
- MOON, J., WALTER, B., AND MARSCHNER, S. 2007. Rendering discrete random media using precomputed scattering solutions. *Rendering Techniques 2007*, 231–242. <https://doi.org/10.2312/EGWR/EGSR07/231-242>.
- MÜLLER, T., PAPAS, M., GROSS, M., JAROSZ, W., AND NOVÁK, J. 2016. Efficient rendering of heterogeneous polydisperse granular media. *ACM Transactions on Graphics (TOG)* 35, 6, 1–14. <https://doi.org/10.1145/2980179.2982429>.

- MUNK, M., AND SLAYBAUGH, R. N. 2019. Review of hybrid methods for deep-penetration neutron transport. *Nuclear Science and Engineering*, 1–35. <https://doi.org/10.1080/00295639.2019.1586273>.
- NICODEMUS, F. E., RICHMOND, J. C., HSIA, J. J., GINSBERG, I. W., AND LIMPERIS, T. 1977. *Geometrical Considerations and Nomenclature for Reflectance*. National Bureau of Standards.
- NOVÁK, J., GEORGIEV, I., HANIKA, J., AND JAROSZ, W. 2018. Monte carlo methods for volumetric light transport simulation. In *Computer Graphics Forum*, vol. 37, Wiley Online Library, 551–576. <https://doi.org/10.1111/cgf.13383>.
- PHARR, M., JAKOB, W., AND HUMPHREYS, G. 2016. *Physically based rendering: From theory to implementation*. Morgan Kaufmann.
- PICARD, É. 1911. Sur un exemple simple d'une équation singulière de fredholm où la nature analytique de la solution dépend du second membre. In *Annales scientifiques de l'École Normale Supérieure*, vol. 28, 313–324. <https://eudml.org/doc/81303>.
- RAAB, M., SEIBERT, D., AND KELLER, A. 2008. Unbiased global illumination with participating media. In *Monte Carlo and Quasi-Monte Carlo Methods 2006*. Springer, 591–605. [https://doi.org/10.1007/978-3-540-74496-2\\_35](https://doi.org/10.1007/978-3-540-74496-2_35).
- RABINOWITCH, E. I. 1951. *Photosynthesis and related processes*, vol. 72. LWW.
- RANDALL, C. H. 1962. Stochastic models for heterogeneous materials. I.(Large scale inhomogeneities and neutron transmission. Tech. Rep. KAPL-M-CHR-6, Knolls Atomic Power Lab., Schenectady, NY.
- RANDALL, C. 1964. Generalized treatment of particle self-shielding. In *The Naval Reactors Handbook Vol. 1: Selected Basic Techniques*, A. Radkowsky, Ed. United States Atomic Energy Comission, 553.
- SIEWERT, C. 1980. On computing eigenvalues in radiative transfer. *Journal of Mathematical Physics* 21, 9, 2468–2470. <https://doi.org/10.1063/1.524684>.
- SPANIER, J., AND GELBARD, E. 1969. *Monte Carlo principles and neutron transport problems*. Addison-Wesley Pub. Co.
- TORQUATO, S. 2016. Hyperuniformity and its generalizations. *Physical Review E* 94, 2, 022122. <https://doi.org/10.1103/PhysRevE.94.022122>.
- TUNALEY, J. 1974. Theory of ac conductivity based on random walks. *Physical Review Letters* 33, 17, 1037. <https://doi.org/10.1103/PhysRevLett.33.1037>.
- TUNALEY, J. 1976. Moments of the Montroll-Weiss continuous-time random walk for arbitrary starting time. *Journal of Statistical Physics* 14, 5, 461–463. <https://doi.org/10.1007/BF01040704>.
- TURNER, S. A., AND LARSEN, E. W. 1997. Automatic variance reduction for three-dimensional Monte Carlo simulations by the local importance function transform–1: Analysis. *Nucl. Sci. Eng.* 127, 1. <https://doi.org/10.13182/NSE127-22>.
- UEKI, T., AND LARSEN, E. W. 1998. A kinetic theory for nonanalog monte carlo particle transport algorithms: Exponential transform with angular biasing in planar-geometry anisotropically scattering media. *Journal of Computational Physics* 145, 1, 406–431. <https://doi.org/10.1006/jcph.1998.6039>.
- VICINI, D., KOLTUN, V., AND JAKOB, W. 2019. A learned shape-adaptive subsurface scattering model. *ACM Transactions on Graphics (TOG)* 38, 4, 1–15. <https://doi.org/10.1145/3306346.3322974>.

- WEISS, G. H. 1983. Random walks and their applications: Widely used as mathematical models, random walks play an important role in several areas of physics, chemistry, and biology. *American Scientist* 71, 1, 65–71. <https://www.jstor.org/stable/27851819>.
- WILLIAMS, M. 1991. Generalized contributon response theory. *Nucl. Sci. Eng.* 108, 355–383. <https://doi.org/10.13182/NSE90-33>.
- WILLIAMS, M. M. R. 2007. The searchlight problem in radiative transfer with internal reflection. *Journal of Physics A: Mathematical and Theoretical* 40, 24, 6407. <https://doi.org/10.1088/1751-8113/40/24/009>.
- WING, G. 1962. *An introduction to transport theory*. Wiley.
- WINSLOW, A. M. 1968. Extensions of asymptotic neutron diffusion theory. *Nuclear Sci. and Eng.* 32, 101–110. <https://doi.org/10.13182/NSE68-A18829>.
- WRENNINGE, M., VILLEMIN, R., AND HERY, C. 2017. Path traced subsurface scattering using anisotropic phase functions and non-exponential free flights. Tech. Rep. 17-07, Pixar. <https://graphics.pixar.com/library/PathTracedSubsurface>.
- XU, Q., SUN, J., WEI, Z., SHU, Y., MESSELODI, S., AND CAI, J. 2001. Zero variance importance sampling driven potential tracing algorithm for global ilumination.
- XU, Q., WANG, W., AND BAO, S. 2006. A new computational way to Monte Carlo global illumination. *International Journal of Image and Graphics* 6, 01, 23–34. <https://doi.org/10.1142/S0219467806002057>.
- ZHAO, S., RAMAMOORTHI, R., AND BALA, K. 2014. High-order similarity relations in radiative transfer. *ACM Transactions on Graphics (TOG)* 33, 4, 104. <https://doi.org/10.1145/2601097.2601104>.
- ZOIA, A., DUMONTEIL, E., AND MAZZOLO, A. 2011. Collision densities and mean residence times for d-dimensional exponential flights. *Physical Review E* 83, 4, 041137. <https://doi.org/10.1103/PhysRevE.83.041137>.